

1 **FRONT MATTER**

2
3 **Title: Temperature-dependent fasciation mutants connect mitochondrial RNA processing**
4 **to control of lateral root morphogenesis**
5

6 **Authors**

7 Kurataka Otsuka^{1†‡}, Akihito Mamiya^{1†}, Mineko Konishi^{1§}, Mamoru Nozaki^{1||}, Atsuko Kinoshita^{1¶},
8 Hiroaki Tamaki^{1#}, Masaki Arita^{1††}, Masato Saito^{1‡‡}, Kayoko Yamamoto^{1§§}, Takushi Hachiya², Ko
9 Noguchi³, Takashi Ueda⁴, Yusuke Yagi⁵, Takehito Kobayashi^{5|||}, Takahiro Nakamura⁵, Yasushi
10 Sato⁶, Takashi Hirayama⁷, Munetaka Sugiyama^{1*}
11

12 **Affiliations**

13 ¹Botanical Gardens, Graduate School of Science, The University of Tokyo, Tokyo, 112-0001,
14 Japan.

15 ²Department of Molecular and Functional Genomics, Interdisciplinary Center for Science
16 Research, Shimane University, Shimane, 690-8504, Japan.

17 ³Department of Applied Life Science, School of Life Sciences, Tokyo University of Pharmacy and
18 Life Sciences, Tokyo, 192-0392, Japan.

19 ⁴Division of Cellular Dynamics, National Institute for Basic Biology, Aichi, 444-8585, Japan.

20 ⁵Department of Bioscience and Biotechnology, Faculty of Agriculture, Kyushu University,
21 Fukuoka, 819-0395, Japan.

22 ⁶Biology and Environmental Science, Graduate School of Science and Engineering, Ehime
23 University, Ehime, 790-8577, Japan.

24 ⁷Institute of Plant Science and Resources, Okayama University, Okayama, 710-0046, Japan.

25 ‡Present address: Division of Molecular and Cellular Medicine, National Cancer Center Research
26 Institute, Tokyo, 104-0045, Japan. / R&D Division, Kewpie Corporation Sengawa Kewport,
27 Tokyo, 182-0002, Japan. / Division of Molecular and Cellular Medicine, Institute of Medical
28 Science, Tokyo Medical University, Tokyo, 160-0023, Japan.

29 §Present address: Biotechnology Research Center, The University of Tokyo, Tokyo, 113-8657,
30 Japan.

31 ||Present address: Biotechnology Research Center and Department of Biotechnology, Toyama
32 Prefectural University, Toyama, 939-0398, Japan.

33 ¶Present address: Department of Biological Sciences, Graduate School of Science, Tokyo
34 Metropolitan University, Tokyo, 192-0397, Japan.

35 #Present address: Health and Crop Sciences Research Laboratory, Sumitomo Chemical Co. Ltd.,
36 Hyogo, 665-8555, Japan.

37 ‡‡Present address: Innovation Promotion Division, Oji Holdings Corporation, Tokyo, 135-8558,
38 Japan.

39 §§Present address: Department of Biological Sciences, Graduate School of Science, Tokyo, 113-
40 0033, Japan.

41 |||Present address: GRA&GREEN Inc., Incubation Facility 106, Nagoya University, Aichi, 464-
42 0814, Japan.

43 †These authors contributed equally to this work.

44 *Corresponding author. Email: sugiyama@ns.bg.s.u-tokyo.ac.jp

45 Abstract

46 Although mechanisms that activate organogenesis in plants are well established, much less
47 is known about the subsequent fine-tuning of cell proliferation, which is crucial for creating
48 properly structured and sized organs. Here we show, through analysis of temperature-
49 dependent fasciation (TDF) mutants of Arabidopsis, *root redifferentiation defective 1*
50 (*rrd1*), *rrd2*, and *root initiation defective 4* (*rid4*), that mitochondrial RNA processing is
51 required for limiting cell division during early lateral root (LR) organogenesis. These
52 mutants formed abnormally broadened (i.e., fasciated) LRs under high-temperature
53 conditions due to excessive cell division. All TDF proteins localized to mitochondria,
54 where they were found to participate in RNA processing: RRD1 in mRNA deadenylation,
55 and RRD2 and RID4 in mRNA editing. Further analysis suggested that LR fasciation in
56 the TDF mutants is triggered by reactive oxygen species generation caused by defective
57 mitochondrial respiration. Our findings provide novel clues for the physiological
58 significance of mitochondrial activities in plant organogenesis.
59
60

61 MAIN TEXT

62 Introduction

63 Plants elaborate their architecture by continuously developing new organs, such as leaves,
64 floral organs, axillary stems, and lateral roots (LRs). Organogenesis begins with the local
65 activation of cell proliferation in the plant body. In the following stages, proliferation is
66 restricted to certain areas, which is essential for the formation of properly sized and
67 structured organs. However, the molecular underpinnings of such regulation remain mostly
68 unknown.

69 LRs serve as building blocks of the root system architecture, and are crucial for the
70 uptake and transport of water and minerals. The first visible step of LR formation occurs
71 within the parent root, where a few cells start to divide, comprising the LR primordium.
72 The LR primordium grows and eventually emerges out of the parent root to form a new
73 LR [1]. This process has been described in detail in the model plant *Arabidopsis thaliana*
74 (*Arabidopsis*), rendering it one of the most ideal systems to study the molecular
75 mechanisms of organ development [3,4]. In *Arabidopsis*, a small number of cells in a few
76 adjacent files of the xylem pole pericycle layer, termed LR founder cells, re-enter the cell
77 cycle and first divide in the anticlinal (perpendicular to the parental root axis) orientation
78 (Fig. 1B) [3,4]. The local accumulation of the phytohormone auxin is critical for LR
79 initiation, driving LR founder cell identity acquisition and division via the degradation of
80 the SOLITARY ROOT (SLR/IAA14) repressor, thus activating the expression of down-
81 stream genes mediated by the AUXIN RESPONSE FACTORS ARF7 and ARF19 [5].
82 However, much less is understood about the coordinated periclinal (parallel to the surface
83 of the root) and anticlinal divisions that subsequently take place. In particular, the manner
84 in which cell proliferation becomes confined to the central zone of the primordium, giving
85 rise to the dome-shaped structure, largely remains a mystery [1], although the requirement
86 of several factors, such as polar auxin transport [6,7], control of auxin response [8], a few
87 peptide hormones [9,10], transcription factors [11,12], symplastic connectivity [13],
88 epigenetic gene regulation [14], and mechanical interaction with the overlaying tissue [15],
89 has been revealed.

90 *root redifferentiation defective 1* (*rrd1*), *rrd2*, and *root initiation defective 4* (*rid4*) are
91 temperature-sensitive mutants of *Arabidopsis* that were originally isolated by us via
92 screening using adventitious root (AR) formation from hypocotyl tissue segments as an

93 index phenotype [16,17]. In addition to AR formation, other aspects of development, such
94 as seedling growth and callus formation, were affected by high-temperature conditions
95 [16,17]. Most notable among these aspects was their LR phenotype, in which abnormally
96 broadened (i.e., fasciated) LRs were formed at 28°C (non-permissive temperature), but not
97 at 22°C (permissive temperature), in a tissue culture setting; thus, we termed the three
98 mutants as temperature-dependent fasciation (TDF) mutants [18]. It was later revealed that
99 the early stages of LR development are likely affected in the TDF mutants, and that the
100 fasciated LRs exhibit exclusive enlargement of inner tissues [18], suggesting that the genes
101 responsible for the TDF mutations (TDF genes) encode negative regulators of proliferation
102 that are important for the size restriction of the central zone during the formation of early
103 stage LR primordia; however, their molecular identity has remained elusive.

104 Plant cells have gene expression systems in mitochondria and plastids in addition to
105 the nucleus. Although organelle gene expression is typically associated with organelle-
106 specific functions, it might also be involved in higher-order physiological activities
107 including the regulation of organogenesis. Mitochondria are considered the “powerhouses”
108 of the cell, as they supply the energy that is necessary for cellular activities. In comparison
109 with other eukaryotes, RNA metabolism in mitochondria is particularly complex in plants,
110 and entails numerous nuclearly encoded RNA-binding proteins [2]. Given the relaxed
111 nature of transcription, post-transcriptional processing, such as RNA editing, splicing,
112 maturation of transcript ends and RNA degradation, are known to play predominant roles
113 in shaping the plant mitochondrial transcriptome [2]. Many factors that participate in plant
114 mitochondrial RNA processing have been identified; however, the implications of their
115 role in regulating plant organ development remain unclear [2].

116 Herein, we report a detailed analysis of the TDF mutants. We found that LR fasciation
117 in the TDF mutants was caused by excessive cell division in the early stages of LR
118 formation. Next, we identified all three TDF genes as encoding nuclearly encoded
119 mitochondrial RNA processing factors. Analysis of mitochondrial RNA demonstrated that
120 RRD1 is involved in the removal of poly(A) tails, and that both RRD2 and RID4 are RNA
121 editing factors. Defective protein composition of the mitochondrial electron transport chain
122 was found in *rrd2* and *rid4*. Phenocopying of the TDF mutants by mitochondrial
123 respiratory inhibition and reactive oxygen species (ROS) induction, together with its
124 reversal by ROS scavenging, suggested that ROS generation resulting from impaired RNA
125 processing is the primary cause of the excessive cell division observed during early LR
126 development in the TDF mutants. Our discovery shed light on a new aspect of
127 mitochondrial RNA processing that is relevant in the control of plant organogenesis.

129 Results

130 Effects of the TDF mutations on LR formation

131 To gain insight into fasciated LR formation in the TDF mutants, a detailed investigation
132 was carried out using the semi-synchronous LR induction system [19], in which nearly de
133 novo LR formation is induced from root explants of young seedlings upon culture in auxin-
134 containing root inducing medium (RIM). In this system, a 6-day culture of TDF mutant
135 explants results in high rates of LR fasciation at 28°C (non-permissive temperature) (Fig.
136 1A), but not at 22°C (permissive temperature) [18]. To determine the stage of LR formation
137 at which developmental abnormalities occur in the TDF mutants, LR primordia from
138 earlier time points were examined. In Arabidopsis, LR formation begins with anticlinal cell
139 divisions in the xylem pole pericycle cell file, producing an array of short cells flanked by

140 longer cells, which serve as the origin of the LR primordium (stage I; Fig. 1B) [3,4]. This
141 is followed by periclinal divisions throughout the primordium, with the exception of the
142 flanking cells in some occasions, creating two cell layers (stage II; Fig. 1B). Subsequent
143 periclinal cell divisions take place in the central zone of the primordium, producing the
144 third cell layer (stage III), followed by the fourth cell layer (stage IV; Fig.1B). Additional
145 anticlinal cell division, together with cell expansion at the innermost cell layer, gives rise
146 to a dome-shaped primordium (stage V; Fig. 1B). The comparison of the number of cells
147 within the area consisting of more than one layer (MOL) [11] between stages II and III,
148 revealed that all TDF mutants showed an increase in this parameter in a temperature-
149 dependent manner (Fig. 1, C to E). The same trend was observed in primordia at stage IV
150 and V, for which the widths of the MOL and more than three layer (MTL) [11] areas were
151 quantified (Fig. 1, F to H). These results showed that TDF mutants exhibit excessive cell
152 division in the initial steps of LR development, namely as early as stage II, and indicate
153 that the increase in the number of cells along the lateral axis of the primordium induces the
154 expansion of its central zone, giving rise to an abnormally broadened and flat-shaped LR.
155 As there was no significant increase in LR density (Fig. 1I; Kruskal-Wallis test, $P > 0.3$),
156 LR fasciation in the TDF mutants seems to be the result of the expansion of individual
157 primordia, as opposed to the fusion of multiple primordia because of overcrowding that is
158 observed in some other mutants [9,13].

159 **Positional cloning and expression analysis of the TDF genes**

160 To clone the TDF genes, we mapped the mutated loci in the TDF mutants based on the
161 temperature-sensitive AR formation phenotype, which originally led to the isolation of the
162 mutants (fig. S1) [16,17]. The candidate genes identified by sequencing the mapped regions
163 were confirmed either by a complementation test (*RRD1* and *RID4*; fig. S2, A and E) or an
164 allelism test (*RRD2*; fig. S2, B to D). This resulted in the identification of *RRD1* as
165 At3g25430, which encodes a poly(A)-specific ribonuclease (PARN)-like protein, and
166 *RRD2* and *RID4* as At1g32415 and At2g33680, respectively, both of which encode a
167 pentatricopeptide repeat (PPR) protein belonging to the PLS subfamily (Fig. 2A).
168 At1g32415 has previously been reported as the gene responsible for the *cell wall*
169 *maintainer 2* (*cwm2*) mutation [20]; thus, we will refer to it as *RRD2/CWM2* henceforth.
170 *rrd1*, *rrd2*, and *rid4-1* are all nonsense mutations (Fig. 2A). The *rrd1* mutation results in
171 an 89-amino-acid C-terminal truncation of the 618-amino-acid RRD1 protein; the mutant
172 protein may be partially or conditionally functional. As the *rrd2* and *rid4* mutations create
173 a stop codon close to the start codon (Fig. 2A), they are likely to eliminate gene function.
174 Later in our study, another mutant harboring a mutation in the *RID4* gene was isolated and
175 designated *rid4-2* (Fig. 2A and fig. S3). *rid4-2* exhibited LR fasciation as well as retarded
176 seedling growth at high-temperature conditions, similar to *rid4-1* (fig. S3, A and B). The
177 *rid4-2* mutation is a missense mutation that gives rise to a single amino acid substitution
178 (G137R) (Fig. 2A and fig. S3D), presumably causing a partial reduction of gene function.

179 GFP reporter studies were carried out to elucidate the expression patterns of the TDF
180 genes. For *RRD1* and *RID4*, genomic constructs encompassing the promoter region to the
181 end of the protein-coding sequence (*RRD1::RRD1:GFP* and *RID4::RID4:GFP*) were
182 generated and introduced into *rrd1* and *rid4-1*, respectively. The suppression of the mutant
183 AR phenotype demonstrated the functionality of the reporter genes (fig. S4, A and B). For
184 both *RRD1* and *RID4*, strong GFP expression was mostly confined to apical meristems and
185 LR primordia in the root system and slightly and much weaker expressions were detected
186 in the stele and cortex/epidermis tissues, respectively (Fig. 2B, and fig. S4C). This
187 resembled the *35S::Mt-GFP* line, which expresses mitochondria-targeted GFP under the
188 constitutive active cauliflower mosaic virus (CaMV) 35S promoter (Fig. 2C). At the

189 subcellular level, fluorescence from the GFP-fusion proteins appeared punctate or
190 granulated and was largely overlapped with signals from the mitochondrion-specific dye
191 MitoTracker Orange, demonstrating that the majority of RRD1 and RID4 proteins are
192 localized to mitochondria (Fig. 2D). Although the tissue-level investigation of
193 *RRD2/CWM2* expression was unsuccessful because of the undetectable levels of the
194 signals of *RRD2::RRD2:GFP*, mitochondrial localization was also confirmed for RRD2
195 by studying transient expression under the 35S promoter (Fig. 2E). Together, these data
196 showed that the TDF genes *RRD1*, *RRD2/CWM2*, and *RID4* encode putative RNA
197 processing factors that localize to mitochondria.

198 **Analysis of the role of RRD1 in poly(A) degradation of mitochondrial mRNAs**

199 PARN belongs to the DEDD superfamily of deadenylases [21]. Recent human and animal
200 studies have led to an increased appreciation of its participation in the maturation process
201 of a wide variety of noncoding RNAs [22]. In plants, however, PARN plays a distinct role
202 in the removal of the poly(A) tails of mitochondrial mRNA [23–25]. Given the sequence
203 similarity to PARN and its mitochondrial localization, we hypothesized that RRD1 is also
204 involved in regulating the poly(A) status of mitochondrial mRNA. To test this possibility,
205 we first performed a microarray analysis of poly(A)⁺ RNAs prepared from wild-type and
206 *rrd1* explants that had been induced to form LRs at 28°C, and found a substantial increase
207 in mitochondria-encoded poly(A)⁺ transcripts in *rrd1* explants (Fig. 3A, and fig. S5, A to
208 C). As the majority of plant mitochondrial transcripts normally lack poly(A) tails,
209 presumably because of swift removal after its addition [26], we suspected that the apparent
210 sharp increase in mitochondrial transcript level might be ascribed to defective poly(A) tail
211 removal, rather than increased transcription. In fact, a comparative analysis of
212 polyadenylated and total RNA levels via quantitative reverse transcription polymerase
213 chain reaction (qRT-PCR) revealed a selective increase in polyadenylated transcripts (Fig.
214 3B). Furthermore, a circularized RNA (CR)-RT PCR analysis [27] of the *cytochrome*
215 *oxidase subunit 1 (cox1)* mRNA was performed to study its 3' extremity, and revealed a
216 marked increase in the polyadenylated to non-polyadenylated ratio in *rrd1* compared with
217 the wild-type plant (Fig. 3C). In addition, a poly(A) test assay by rapid amplification of
218 cDNA ends (RACE-PAT) [28] showed that polyadenylated transcript levels were
219 increased at higher temperature in *rrd1* (Fig. 3D). Taken together, these results
220 demonstrated that RRD1 is involved in poly(A) tail removal in mitochondrial mRNAs, and
221 that, in *rrd1*, polyadenylated mitochondrial transcripts accumulate in a temperature-
222 dependent manner.

223 Next, we investigated whether the RRD1 protein itself has deadenylation activity. In
224 previous studies, this possibility was excluded because, in contrast to canonical PARNs
225 (including AtPARN/AHG2), RRD1 lacks three out of the four amino acids that are
226 essential for its function as a deadenylase [29]. In our assay, as expected, the recombinant
227 RRD1 protein did not show any activity in the conditions effective for human PARN (fig.
228 S5, D and E). We concluded that the RRD1 protein alone does not have deadenylase
229 activity.

230 To assess the effects of the observed accumulation of poly(A)⁺ mitochondrial
231 transcripts in *rrd1*, we introduced the *ahg2-1* suppressor 1 (*ags1*) mutation into *rrd1*. *ags1*
232 is a mutation of a mitochondrion-localized poly(A) polymerase (PAP), AGS1, which was
233 originally identified based on its ability to counteract AtPARN/AHG2 loss of function [23].
234 A substantial decrease in mitochondrial poly(A)⁺ transcript levels was observed in the *rrd1*
235 *ags1* double mutant compared with the *rrd1 AGS1* control (Fig. 4A). Moreover, *rrd1*
236 phenotypes, such as temperature-dependent LR fasciation and seedling growth retardation,

237 were significantly alleviated (Fig. 4, B and C). These results indicate that the accumulation
238 of poly(A)⁺ mitochondrial transcripts is the primary cause of the *rrd1* phenotype.

239 **Analysis of the roles of RRD2 and RID4 in mitochondrial mRNA editing**

240 PPR proteins are known for their role in regulating various aspects of organellar post-
241 transcriptional gene expression, such as RNA stabilization, RNA cleavage, RNA splicing,
242 RNA editing, and translation [2,30]. They are characterized by the tandem assembly of
243 degenerate protein motifs of about 35 amino acids, termed PPR motifs [30]. The PPR
244 motifs allow PPR proteins to recognize specific sites of single-stranded RNAs through a
245 one-motif to one-base interaction [30]. The PPR protein family has undergone a
246 remarkable expansion in land plants, representing one of the largest protein families thereof
247 [30]. RRD2 and RID4 belong to the PLS-class of PPR proteins, most of which have been
248 reported as being C-to-U RNA editing factors [31]. The PLS class PPR proteins contain
249 three types of PPR motifs, the P motif (normally 35 a. a. in length), the L motif (35–36 a.
250 a. (long)) and the S motif (31 a. a. (short)), in contrast to the P-class PPR proteins, which
251 only contain P motifs [30,32]. Considering their localization to mitochondria (Fig. 2, D and
252 E), we speculated on the involvement of RRD2 and RID4 in the editing of mitochondrial
253 RNA. A comprehensive sequence analysis of previously reported RNA editing sites using
254 cDNA prepared from explants induced to form LR_s at 28°C revealed an almost complete
255 abolishment of C-to-U editing at two sites (*cytochrome c biogenesis protein 2 (ccb2)*-71C
256 and *ccb3*-575C) in *rrd2* and at six sites (*ATP synthase subunit 4 (atp4)*-395C, *ribosomal*
257 *protein l5 (rpl5)*-58C, *rpl5*-59C, *rps3*-1344C, *rps4*-77C, and *rps4*-332C) in *rid4* (Fig. 5A,
258 fig. S7). The identification of *ccb3*-575C as an RRD2/CWM2 editing site was in agreement
259 with a previous study of *cwm2* [20]. Editing was also completely abolished in these sites
260 at 22°C (fig. S8A). RID4 editing sites showed incomplete editing in *rid4-2*, implying a
261 partial loss of function in this mutant (fig. S7). Significant identity was found among the
262 5' upstream sequences of the editing sites that were affected in each mutant (fig. S8B),
263 further suggesting that RRD2 and RID4 participate in the editing of these sites via direct
264 contact.

265 In addition, all editing sites of *ccb3*, with the exception of those that were unedited in
266 the wild type, showed declining levels of RNA editing in both *rrd2* and *rid4* (fig. S7).
267 However, these sites were not considered as targets of RRD2 and RID4 for the following
268 reasons. These sites were incompletely edited, even in the wild type, as opposed to most
269 other sites (fig. S7), suggesting that their editing is relatively slow and highly susceptible
270 to fluctuations in the kinetic balance between editing and transcription. Moreover, editing
271 at these sites was almost unaffected at 22°C (fig. S8C) and was only partially inhibited at
272 28°C in *rrd2* and *rid4* (fig. S7), even though these mutants are assumed to have lost the
273 function of the corresponding genes completely. *ccb3*-624C was also not regarded as a
274 target site, despite the complete absence of editing in both *rrd2* and *rid4*, as it was more
275 likely due to originally low levels of editing compared with other sites in *ccb3* (fig. S7).
276 This view was reinforced by the lack of similarity in the upstream sequence between *ccb3*-
277 624C and the other editing sites that were strongly affected by the *rrd2* and *rid4* mutations
278 (fig. S8B).

279 Next, to investigate the effects of losses of function of RRD2/CWM2 and RID4 on
280 mitochondrial protein composition, we performed a blue-native (BN)-PAGE analysis of
281 mitochondrial extracts prepared from seed-derived callus cultured for 3 days at 22°C or
282 28°C after a 20-day 22°C incubation period. This revealed a substantial loss of complex V
283 (ATP synthase complex) in *rid4* at both 22°C and 28°C culture conditions (Fig. 5B), likely
284 caused by defective mRNA editing of *atp4* (Fig. 5A), which is a component of this protein

285 complex. No noticeable differences were found in *rrd1* and *rrd2*. Because *ccb2* and *ccb3*,
286 the two mitochondrial genes that are targeted by RRD2/CWM2, are related to cytochrome
287 c (cyt c) maturation [33], we quantified cyt c levels in *rrd2*. Cyt c levels on a per
288 mitochondrial protein basis were decreased in *rrd2* callus cultured at 28°C for 3 days (Fig.
289 5, C and D) in two out of three cultures, although the difference was not significant when
290 all three results were included. This decrease in cyt c levels in *rrd2* was in accordance with
291 a previous analysis of *cwm2* [20]. At 22°C, however, no significant difference was
292 observed between *rrd2* and the wild type. Furthermore, we found that the difference in cyt
293 c levels was more pronounced after longer periods of culture at 28°C (Fig. 5, E and F).
294 These results indicate that, in *rrd2*, cyt c maturation activity was affected to a greater extent
295 at higher temperatures, at least in callus, which possesses root-tissue-like properties,
296 possibly explaining the temperature-dependent nature of its phenotype. The data reported
297 above demonstrated that, in both *rrd2* and *rid4*, the production of certain components of
298 the mitochondrial electron transport chain is hampered by defective mRNA editing.

299 **Effects of defective mitochondrial respiration on LR formation**

300 Based on the results obtained for *rrd1*, *rrd2*, and *rid4*, we speculated that there might be a
301 relationship between mitochondrial electron transport and cell division control during LR
302 morphogenesis. In fact, the induction of LRs from wild-type explants in the presence of
303 rotenone (complex I inhibitor), antimycin A (complex III inhibitor), or oligomycin
304 (complex V inhibitor) led to LR fasciation, providing evidence that electron transport chain
305 defects are the cause of the TDF LR phenotype (Fig. 6, A to D). To further investigate the
306 underlying molecular pathway, we next asked whether either reduced ATP synthesis, or
307 ROS generation, phenomena that are commonly associated with defective mitochondrial
308 respiration might be involved. We found that the respiratory uncoupler carbonylcyanide
309 m-chlorophenyl-hydrazone (CCCP) did not increase LR width (Fig. 6E), although LR
310 growth inhibition was observed in a dose-dependent manner (Fig. 6F), whereas the ROS
311 inducer paraquat (PQ) triggered a significant fasciation of LRs (Fig. 6, G and H).
312 Furthermore, the application of the ROS scavenger ascorbate resulted in a reversal of the
313 LR broadening induced by PQ treatment (Fig. 6, G and H). The same effect was observed
314 against the *rid4-2* mutation. These data suggest that the increase in the levels of ROS, but
315 not the decrease in the levels of ATP, acts downstream of defective mitochondrial
316 respiration to promote excessive cell division during LR development in the TDF mutants.

317 Local gradient formation of auxin is important for LR initiation and the subsequent
318 organization of the LR primordium [5–7]. Strong genetic perturbations of polar auxin
319 transport result in homogeneous proliferation of the pericycle cell layer in large regions of
320 the root upon exogenous auxin treatment. In addition, chemical inhibition of auxin polar
321 transport by naphthylphthalamic acid (NPA) gave rise to broadened LR primordia
322 reminiscent of fasciated LRs of the TDF mutants (fig. S9). These data indicate a role for
323 local auxin gradient formation in restricting proliferative capacity during LR formation.
324 Therefore, we tested whether ROS-induced LR fasciation is mediated by altered auxin
325 patterning in early LR primordia. The examination of the expression pattern of the auxin-
326 responsive β -glucuronidase marker *DR5::GUS* [6–8] at early stages of LR induction,
327 however, did not reveal differences between the control and PQ-treated root segments,
328 whereas treatment with NPA resulted in enhanced expression along the entire root segment
329 (Fig. 6I). This result indicates that ROS-induced LR fasciation is not caused by an
330 impairment in auxin gradient formation.

331
332

333 Discussion

334 In the present study, we investigated three TDF mutants of Arabidopsis, *rrd1*, *rrd2*, and
335 *rid4*, which form fasciated LR s at high temperatures, and identified mutations in previously
336 poorly characterized genes encoding mitochondria-localized proteins as being responsible
337 for the phenotype of these mutants. Our results elucidated the roles of these genes in
338 mitochondrial RNA processing, the construction of the respiratory chain, and in the
339 restrictive control of cell proliferation during LR primordium development.

340 Excessive cell division during early primordium development leads to LR fasciation

341 In the present study, we investigated the formation of fasciated LR s observed at high-
342 temperature conditions in the TDF mutants using the semi-synchronous LR induction
343 system [19]. By measuring the cell number and primordium width, we found that fasciation
344 of LR s is caused by excessive anticlinal cell division, which takes place as early as stage
345 II of LR development (Fig. 1). The lack of increase in LR density (Fig. 1I) suggested that
346 LR fasciation is caused by the expansion of individual primordia, rather than the fusion of
347 multiple primordia, which is the case in some other mutants that form abnormally
348 broadened LR s [9,13]. The data are in agreement with the previous result of the
349 temperature-shift experiment, which demonstrated that the first 48 h following LR
350 induction are critical for LR fasciation in the TDF mutants [18], as stage II to early stage
351 III primordia are formed within this time frame (Fig. 2D) [19]. The previous
352 characterization of the TDF mutants also showed that fasciated LR primordia exhibit
353 specific enlargement of inner root tissues marked by the expression of *SHORT ROOT*
354 (*SHR*), while the number of cell layers outside the *SHR*-expressing layer is normal [18]. A
355 recent study revealed that the area of *SHR* expression is first established during stage II,
356 where it is confined to the inner layer of the two-cell layered primordium [4]. In subsequent
357 stages, *SHR* is expressed in cell files derived from the inner layer, which develop into the
358 stele of the LR [4]. Taken together, these results suggest that differentiation into two cell
359 layers at stage II occurs normally in the TDF mutants, and that the increase in the number
360 of cells observed at stage II consequently leads to the expansion of the area of *SHR*
361 expression in the inner cell layer during LR fasciation.

362 RRD1 functions in poly(A) tail removal in mitochondrial mRNA

363 PARN is a 3' exoribonuclease of the DEDD superfamily [21], which shows a strong
364 preference for adenine [21,22]. In plants, PARN is involved in the removal of poly(A) tails
365 from mitochondrial transcripts [23–25]. Here, we identified *RRD1* as a gene encoding a
366 PARN-like protein (Fig. 2A) that resides in mitochondria (Fig. 2, B and C). Further
367 analysis of *rrd1* demonstrated the participation of RRD1 in poly(A) tail degradation of
368 mitochondrial mRNA (Fig. 3). In plant mitochondria, immature 3' extremities of mRNA,
369 together with irregular RNAs, such as 3' misprocessed mRNAs, rRNA maturation by-
370 products, and cryptic transcripts, are known to be polyadenylated before they are degraded
371 by mitochondrial polynucleotide phosphorylase (mtPNPase) [26]. In fact, down-regulation
372 of mtPNPase in Arabidopsis results in the accumulation of long preprocessed mRNAs, as
373 well as irregular RNAs, the majority of which are polyadenylated [26]. In *rrd1*, unusually
374 long preprocessed mRNAs do not seem to accumulate, as the size of RACE-PAT assay
375 products (Fig. 3D) corresponded to that of previously reported mature transcript 3' ends.
376 Total mitochondrial mRNA levels were unelevated in *rrd1* (Fig. 3B), suggesting that
377 RRD1 is not involved in controlling mRNA abundance by promoting their degradation.
378 Whether by-product accumulation takes place in *rrd1* is not clear. However, given its
379 absence in *ahg2* [23], this is unlikely. Based on these considerations, we concluded that

380 RRD1 plays a distinct role from mtPNPase and seems to be specifically involved in 3'
381 processing of near-matured mRNA.

382 The mode of action of the RRD1 protein remains to be solved. The absence of three
383 out of the four catalytic amino acids (DEDD) that are essential for ribonuclease activity
384 (fig. S6) [29], together with the apparent lack of deadenylase activity of the recombinant
385 RRD1 protein (fig. S5, D and E), indicated that RRD1 requires additional factors for its
386 participation in poly(A) tail removal.

387 Failure in the removal of poly(A) tails from mitochondrial transcripts seems to be the
388 primary cause of the *rrd1* phenotype. This is evidenced by the alleviation of the *rrd1*
389 phenotype by the introduction of a mutation of the mitochondria-localized poly(A)
390 polymerase gene *AGS1* (Fig. 4). As most protein-coding genes in the Arabidopsis
391 mitochondrial genome are involved in the biogenesis of the electron transport chain [2], it
392 is likely that mitochondria of *rrd1* carry defects in respiratory activity. However, the exact
393 impact of the altered poly(A) status of mRNAs in mitochondria on electron transport in
394 *rrd1* remains unclear. Unlike the AtPARN/AHG2 loss-of-function mutant *ahg2*, which
395 shows a reduction in complex III levels [23], no significant difference in respiratory chain
396 composition has been detected in *rrd1* to date (Fig. 5B).

397 **RRD2 and RID4 function in mitochondrial mRNA editing**

398 Our study identified *RRD2* and *RID4* as At1g32415 and At2g33680, respectively, both of
399 which encode a mitochondria-localized PLS-class PPR protein (Fig. 2). At1g32415 had
400 previously been reported as the gene responsible for the *cwm2* mutant [20]. A predominant
401 role for PLS-class PPR proteins in RNA editing has been demonstrated with more than 50
402 out of a total of approximately 200 of these proteins in Arabidopsis having been identified
403 as C-to-U editing factors of mitochondria or plastid RNA [31]. A comprehensive analysis
404 of mitochondrial RNA editing revealed the abolishment of editing at specific sites in *rrd2*
405 and *rid4* (Fig. 5A and fig. S7). We concluded that both *RRD2/CWM2* and *RID4* are PLS-
406 class PPR proteins that are involved in mitochondrial mRNA editing.

407 In *rrd2*, editing at 71C of *ccb2* and 575C of *ccb3* was absent (Fig. 5A). Both *ccb2* (also
408 known as *ccb206*, *ccmB*, *ABCI2*, and *AtMg00110*) and *ccb3* (also known as *ccb256*, *ccmC*,
409 *ABCI3*, and *AtMg00900*) encode a multisubunit ATP-binding cassette (ABC) protein,
410 which are involved in the maturation of mono hemic c-type cytochromes, the soluble cyt
411 c, and the membrane-bound cyt c₁ of complex III [33]. Of the two editing sites, *ccb3*-575C
412 was previously reported as a target of *RRD2/CWM2* [20], whereas *ccb2*-71C is a newly
413 discovered target. A decrease in the level of cyt c was detected in *rrd2*, which is consistent
414 with that reported previously for *cwm2* [20]. The data demonstrated the role of
415 *RRD2/CWM2* in cyt c maturation via the RNA editing of cyt c biogenesis factors.

416 In *rid4*, we observed striking reductions in RNA editing at *atp4*-395C, *rpl5*-58, *rpl5*-
417 59C, *rps3*-1344C, *rps4*-77C, and *rps4*-332C. *atp4* (also known as *orf25*, *AtMg00640*)
418 encodes the peripheral stalk protein (subunit b) of the mitochondrial ATP synthase
419 complex (complex V) [34]. *rpl5*, *rps3*, and *rps4* encode mitochondrial ribosome proteins.
420 Analysis of mitochondrial protein complexes showed a dramatic decrease in the level of
421 complex V in *rid4*, probably because of impaired editing of *atp4*-395C. This is similar to
422 the *organelle transcript processing 87* (*otp87*) mutant of Arabidopsis, in which editing of
423 *atp1*-1178C is deficient [35]. These data showed that the formation of complex V could be
424 disrupted by defective RNA editing at a single site of a subunit gene. Considering that the
425 C-to-U editing of the *rps4* transcript at a different site (*rps4*-377) has been shown to affect

426 mitochondrial ribosome assembly in the *growing slowly 1* (*grs1*) mutant [35], it is possible
427 that the *rid4* mutation also has an impact on the mitochondrial ribosome.

428 Recent advances in the mechanistic understanding of RNA binding by PLS-class PPR
429 proteins have led to the identification of residues at certain positions within the PPR motifs
430 that are important for ribonucleotide recognition [30,31]. By mapping these residues of
431 previously reported RNA-editing PPR proteins to their binding sites, which are located 5'
432 upstream of the editing sites, the so-called 'PPR code' has been elucidated, thus enabling
433 the matching of PPR proteins to their candidate editing targets, and vice versa [31].
434 According to the recently refined PPR code prediction [31], RID4 was highly ranked as a
435 potential binding protein of *atp4-395C* (18th, $P = 4.35 \times 10^{-2}$), *rpl5-58C* (5th, $P = 3.04 \times$
436 10^{-2}) and *rps4-332C* (2nd, $P = 4.06 \times 10^{-3}$). Conversely, these sites were among the
437 predicted editing sites of RID4 ($P < 0.05$) [31]. With regard to RRD2, however, the newly
438 identified binding site (*ccb2-71C*) ranked very low, despite the incorporation of
439 RRD2/CWM2 binding to *ccb3-575C* as learning data for the PPR code prediction [31].
440 This discrepancy may be related to the unusual arrangement of PPR motifs in RRD2, in
441 which repeats of SS motifs are prevalent, in contrast to canonical PLS-class PPRs, which
442 follow the (P1-L1-S1)_n-P2-L2-S2 pattern, such as RID4 (Fig. 2A) [32]. Nevertheless, given
443 the similarity between the upstream sequences of editing sites which are severely affected
444 by *rrd2* and *rid4* (fig. S8B), they are likely edited by RRD2 and RID4 via direct interaction.
445 The presented data will contribute to the improvement of PPR protein target estimation.

446 **The origins of the temperature sensitivity may differ among the TDF mutants**

447 A distinct feature of the TDF phenotype is its exclusive observation at high-temperature
448 conditions [16–18]. Our study revealed some differences in the origin of temperature
449 sensitivity among the TDF mutants. The *rrd1* mutation causes a truncation of the C-
450 terminal domain of the RRD1 protein (Fig. 2A). This finding, together with the
451 enhancement of poly(A)⁺ mitochondrial mRNA accumulation at elevated temperatures
452 (Fig. 3D), implies that, in *rrd1*, RRD1 is partially functional at least at the permissive
453 temperature, and that its activity is more severely affected at the non-permissive
454 temperature. In contrast, the *rrd2* and *rid4-1* mutations introduce a stop codon close to the
455 N-terminus of RRD2 and RID4, respectively, likely resulting in the total loss of their
456 functions (Fig. 2A). The complete abolishment of RNA editing of the RRD2 and RID4
457 target sites in the *rrd2* and *rid4-1* mutants, regardless of temperature (Fig. 5A and fig. S8A),
458 further supported this idea. However, in *rrd2*, deficient *cyt c* biogenesis was observed only
459 at high temperature (Fig. 5, C and D). This might be accounted for by the temperature
460 sensitivity of the function of either *ccb2* or *ccb3*, which exhibit alteration of the amino acid
461 sequence in *rrd2*, because of impaired RNA editing (Fig. 5A). In *rid4-1*, a huge reduction
462 in complex V biosynthesis was observed both at permissive and non-permissive
463 temperatures (Fig. 5B). These results suggest that complex V deficiency is more
464 deleterious at higher temperatures, which can explain the temperature sensitivity of the LR
465 fasciation phenotype of *rid4-1*.

466 **Impaired mitochondrial electron transport causes LR fasciation likely via ROS 467 production**

468 The phenocopy of the LR fasciation phenotype of the TDF mutants by treatment with
469 respiratory inhibitors demonstrated the causal relationship between defective
470 mitochondrial electron transport and excessive cell division during early LR development
471 (Fig. 6, A to D). Mitochondrial electron transport is best known for its role in driving ATP
472 synthesis through oxidative phosphorylation. Given the lack of LR fasciation after

473 treatment with the mitochondrial uncoupler CCCP (Fig. 6, E and F), reduced ATP
474 production seems unlikely to be the cause of LR fasciation. The fact that the huge reduction
475 in complex V levels observed in *rid4* (Fig. 5B) does not lead to LR fasciation at the
476 permissive temperature [18] is also supportive of this idea. Experiments using the ROS
477 inducer PQ and the antioxidant ascorbate (Fig. 6, G and H) pointed to mitochondrial ROS
478 generation as the potential trigger of LR fasciation. A previous study also observed
479 enhanced cell division after the application of another ROS inducer, alloxan, during auxin-
480 induced LR formation [36]. In agreement with this ‘ROS hypothesis’, all three respiratory
481 inhibitors used in our study (rotenone, antimycin A, and oligomycin) are potent inducers
482 of oxidative stress [37].

483 ROS have been implicated in stress-induced morphogenic responses (SIMR) [38].
484 Several studies have shown the involvement of phytohormonal regulation in ROS-
485 triggered SIMR. Altered auxin levels and/or distribution have been proposed as potential
486 mediators in the modulation of cell proliferation in response to oxidative stress [36,38].
487 Several recent studies have found antagonistic interactions between auxin signaling and
488 mitochondrial ROS [39]. Auxin is a critical factor in LR development, and the centripetal
489 auxin-gradient formation in early-stage LR primordia is thought to contribute to the
490 organization of the LR primordium [6,7]. However, neither the pattern nor the intensity of
491 the auxin response visualized by the *DR5::GUS* reporter seemed to be altered under PQ
492 treatment, in contrast to the diffuse pattern observed after the application the auxin polar
493 transport inhibitor NPA (Fig. 6I). This indicates that ROS-induced LR fasciation is not
494 attributable to a failure in auxin-gradient formation. Further studies of LR fasciation caused
495 by oxidative stress will elucidate novel aspects of the control of cell proliferation during
496 plant organogenesis.

497 **Mitochondrial RNA processing is linked to the control of cell proliferation**

498 Mutants of nuclearly encoded mitochondrial RNA processing factors have proven to be
499 useful in probing the physiological roles of mitochondrial gene expression. In particular,
500 studies of C-to-U editing PPR protein genes have led to a collection of about 100 mutants,
501 among which RNA-editing mutants are available for most mitochondrial genes [35]. The
502 majority of the mutations confer visible phenotypes, such as growth retardation, impaired
503 embryo development, late flowering, or reduced pollen sterility [35]. Similar
504 developmental defects are also observed in mutants of genes encoding other mitochondrial
505 proteins, including *ndufs4* (complex I mutant), *rpoTnp* (RNA polymerase mutant), and
506 *atphb3* (prohibitin mutant) [40]. These results suggest that mitochondria play a supportive
507 role in plant growth, presumably by supplying energy through oxidative phosphorylation.
508 In this study, however, we found that mitochondrial RNA processing is required for
509 preventing excessive cell division during LR primordium formation. This suggests that
510 mitochondrial gene expression not only supports active cell proliferation for growth and
511 development but also participates in the local fine-tuning of organ morphogenesis by
512 restricting cell proliferation.

513 In summary, our study identified an unexpected link between mitochondrial RNA
514 processing and the control of cell proliferation at the early stage of LR development,
515 probably mediated by changes in the level of mitochondrial ROS. This finding provides a
516 novel clue for the physiological significance of mitochondrial activities in the restrictive
517 regulation of cell proliferation required for the proper morphogenesis of plant organs.

518

519 **Materials and Methods**

520 **Plant materials and growth condition**

521 *Arabidopsis thaliana* (L.) Heynh. ecotypes Columbia (Col) and Landsberg *erecta* (*Ler*)
522 were used as *Arabidopsis* in this work. The TDF mutants *rrd1*, *rrd2*, and *rid4-1* were
523 described previously [16–18]. The *ags1* mutant (*ags1-1*) was also described previously
524 [23]. The *35S::Mt-GFP* line was a gift from Shin-ichi Arimura [41]. *rid4-2* was derived
525 from an ethyl methanesulfonate-mutagenized population of the *Ler* strain of *Arabidopsis*.
526 SALK_027874 was obtained from the *Arabidopsis* Biological Resource Center. *rrd1*
527 mutant strains harboring either *ags1* or *AGSI^c* were obtained by *rrd1* (*Ler* background) ×
528 *ags1* (Col background) and *rrd1* × Col crosses, respectively. The *DR5::GUS* line [42] was
529 a gift from Tom J. Guilfoyle and was crossed three times to *Ler* before use. Primers for the
530 genotyping the mutants are listed in table S1.

531 For tissue culture experiments, donor plants were aseptically grown on Murashige–
532 Skoog medium supplemented with 1.0% (w/v) sucrose, buffered to pH 5.7 with 0.05%
533 (w/v) 2-morpholinoethanesulfonic acid (MES), and solidified with 1.5% (w/v) agar under
534 continuous light ($10\text{--}15\ \mu\text{mol m}^{-2}\ \text{s}^{-1}$) at 22°C. For observation of seedling phenotypes,
535 plants were aseptically grown on the same medium solidified with 1.5% (w/v) agar or 0.8%
536 (w/v) gellan gum under continuous light ($50\text{--}80\ \mu\text{mol m}^{-2}\ \text{s}^{-1}$) at 22°C or 28°C. For self-
537 propagation and crossing, plants were grown on vermiculite under continuous light
538 (approximately $50\ \mu\text{mol m}^{-2}\ \text{s}^{-1}$) at 22°C unless otherwise indicated.

539 **LR induction**

540 As described previously [19], explants were prepared from 4-day-old seedlings grown on
541 agar plates, and cultured on root-inducing medium (RIM) under continuous light ($15\text{--}25$
542 $\mu\text{mol m}^{-2}\ \text{s}^{-1}$) for the induction of semi-synchronous formation of LR. RIM was B5
543 medium supplemented with 2.0% (w/v) glucose and 0.5 mg l⁻¹ indole-3-butyric acid,
544 buffered to pH 5.7 with 0.05% (w/v) MES, and solidified with 0.25% (w/v) gellan gum.
545 Culture temperature was set to 22°C for the permissive condition and to 28°C for the non-
546 permissive condition.

547 **Histological analysis**

548 For whole-mount observation, tissue samples were fixed in 25 mM sodium phosphate
549 buffer (pH 7.0) containing 2% (w/v) formaldehyde and 1% (w/v) glutaraldehyde, rinsed
550 with 100 mM sodium phosphate buffer (pH 7.0), and cleared with an 8:1:2 (w/v/v) mixture
551 of chloral hydrate, glycerin, and water. Observations were made with a microscope
552 equipped with Nomarski optics (BX50-DIC; Olympus) to obtain differential interference
553 contrast (DIC) images.

554 For morphometric analysis of LR primordia, in order to highlight cell organization, the
555 method of [43] was instead employed for tissue fixation and clearing. Developmental
556 stages of LR primordia were determined according to [43]. LR primordia at Stages II to
557 early III and at Stages IV to V were chosen from samples that had been collected after 16
558 to 24 hours and 24 to 48 hours of culture in the semi-synchronous root induction system,
559 respectively, and were measured for their width and cell number.

560 For histochemical detection of GUS reporter expression, tissue samples were fixed in
561 90% (v/v) acetone overnight at -20°C, rinsed with 100 mM sodium phosphate (pH 7.0),
562 and incubated in X-Gluc solution [$0.5\ \text{mg ml}^{-1}$ 5-bromo-4-chloro-3-indolyl β -D-
563 glucuronide cyclohexylammonium salt, 0.5 mM potassium ferricyanide, 0.5 mM

564 potassium ferrocyanide, 100 mM sodium phosphate (pH 7.4)] for 140 min at 37 °C. After
565 rinsing with 100 mM sodium phosphate buffer (pH 7.0), the samples were mounted on
566 glass slides with an 8:1:2 (w/v/v) mixture of chloral hydrate, glycerin, and water, and then
567 subjected to DIC microscopy.

568 **Chromosome mapping**

569 The TDF mutants in the *Ler* background were crossed with the wild-type Col strain, and
570 the resultant F₁ plants were self-pollinated to produce F₂ seeds or test-crossed with the
571 mutant plants to produce TC₁ seeds. The TC₂ lines were then developed by separately
572 collecting self-pollinated progenies from each individual TC₁ plant. F₂ plant or TC₂ lines
573 were checked for the ability of AR formation at 28°C and for DNA polymorphism between
574 *Ler* and Col. Chromosome locations of the TDF mutations were determined on the basis
575 of linkage between the mutations and the *Ler* alleles of polymorphic marker loci.

576 **Identification of the TDF genes**

577 Sequencing of the genomic regions to which the TDF mutations were mapped led to
578 identification of candidates of *RRD1*, *RRD2*, and *RID4* as At3g25430, At1g32415, and
579 At2g33680, respectively. Identification of these genes was confirmed by the
580 complementation test or the allelism test as described below.

581 For the complementation test, genomic clones GL07, encompassing At3g25430 (2.9-
582 kbp 5'-flanking sequence, 2.6-kbp coding sequence, and 2.5-kbp 3'-flanking sequence),
583 and GL91321, encompassing At2g33680 (1.8-kbp 5'-flanking sequence, 3.5-kbp coding
584 sequence, and 2.0-kbp 3'-flanking sequence), were isolated from a transformation-
585 competent genome library [19], and introduced into the *rrd1* and *rid4* mutants, respectively.
586 The resultant transformants were examined for the ability of AR formation at 28°C. To
587 determine allelism between *rrd2* and SALK_027874, which carries a T-DNA insertion in
588 At1g32415, F₁ progeny derived by crossing *rrd2* with SALK_027874 was examined for
589 the ability of AR formation at 28°C.

590 **Plasmid construction**

591 Genomic DNA from *Ler* was used as a template for PCR-based amplification of DNA
592 fragments of interest. *RRD1::RRD1:GFP* was constructed by inserting the -2780/+2495
593 region of the *RRD1* gene (+1 = the first base of the translation initiation codon), which
594 encompassed the genomic region from the promoter to the end of the protein-coding
595 sequence, and the coding sequence of sGFP into pGreen0029 (John Innes Centre).
596 *RID4::RID4:GFP* was similarly constructed by inserting the -2297/+2181 region of the
597 *RID4* gene and the sGFP-coding sequence into pGreen0029. For the construction of
598 *35S::RRD2:GFP*, the +1/+2283 region of the *RRD2* gene was inserted into the pSHO1
599 vector, a derivative of pHTS13 [44]. Plasmids for the PARN activity assay were
600 constructed by inserting the coding sequence of RRD1 or human PARN (hPARN) into the
601 pHAT vector (Clontech). The hPARN sequence was derived from the GNP Human cDNA
602 clone IRAK071M01 (RIKEN BioResource Research Center). In this plasmid construction,
603 the N-terminal mitochondrial localization signal (24 a.a.) sequence was deleted from the
604 RRD1 coding sequence, and the SEP-tag C9D sequence [45] was added to the C-terminus
605 of both RRD1 and hPARN sequences to improve the solubility of these protein products.

606 **Plant transformation**

607 DNAs such as reporter gene constructs and genomic fragments were transformed into
608 *Agrobacterium tumefaciens* and then into Arabidopsis by the floral dip method [46] or its

609 modified version [47]. Transgenic plants were selected by antibiotic resistance and
610 genotyped by PCR for the introduction of the correct transgene. Transient expression of
611 *35S::RRD2:GFP* in protoplasts of cultured cells were done as described in [44].

612 **Expression and localization analysis of GFP reporters**

613 Expression patterns of *RRD1* and *RID4* were examined with transgenic plants harboring
614 *RRD1::RRD1:GFP* and *RID4::RID4:GFP*, respectively. Roots of 6-day-old seedlings of
615 these plants were counterstained with 10 mg l⁻¹ of propidium iodide and fluorescence
616 images were obtained using a confocal microscope (FV3000; Olympus). Expression
617 analysis of *35S::Mt-GFP* was performed in the same conditions using a different confocal
618 microscope (FV1200; Olympus). To investigate subcellular localization of the *RRD1* and
619 *RID4* proteins, protoplasts were prepared from calli that had been induced from the
620 *RRD1::RRD1:GFP* and *RID4::RID4:GFP* explants. The protoplasts were incubated with
621 100 nM Mitotracker Orange (Invitrogen) for 15 minutes to visualize mitochondria and then
622 observed using the LSM710 system (Carl Zeiss).

623 **Microarray analysis and data processing**

624 For microarray analysis, total RNA was extracted with TRIzol reagent (Invitrogen) from
625 explants that had been cultured on RIM for 12 hours in the semi-synchronous LR induction
626 system and purified using the RNeasy microkit (QIAGEN). Affymetrix ATH1 microarrays
627 were hybridized with biotinylated cRNA targets prepared from the RNA samples
628 according to the manufacturer's instructions. It should be noted here that all the targets
629 were derived from poly(A)⁺ RNA in principal because the T7-oligo(dT)₂₄ primer was used
630 for reverse-transcription at the first step of target preparation. Experiments were performed
631 in biological triplicates. The data sets obtained were processed with a variant of MAS5.0
632 utilizing robust radius-minimax estimators [48]. Differential gene expression was
633 identified by RankProd 2.0 [49]. The details of the microarray data was deposited in the
634 Gene Expression Omnibus (<http://www.ncbi.nlm.nih.gov/geo/>) under accession number
635 GSE34595.

636 **Analysis of mRNA polyadenylation status with RACE-PAT**

637 RACE-PAT was performed principally according to [28]. Total RNA was extracted with
638 TRIzol reagent (Invitrogen) either from LR-induced explants or seedlings. Total RNA was
639 treated with RNase-free DNase I (Promega) to eliminate genomic DNA, and reverse-
640 transcribed with T7-oligo(dT)₂₄ as a primer using the PrimeScript II 1st strand cDNA
641 Synthesis kit (TaKaRa). Then the poly(A) tail status was analyzed by PCR with a
642 combination of gene-specific and T7 promoter primers. The thermal cycling program
643 consisted of initial 2-minute denaturation at 95°C followed by 30 cycles of 20 seconds at
644 95°C, 20 seconds at 57°C, and 10 seconds at 72°C. Primers for the RACE-PAT are listed
645 in table S1.

646 **qRT-PCR analysis**

647 For qRT-PCR, total RNA was extracted with TRIzol reagent (Invitrogen) from explants
648 LR-induced at 28°C for 12 hours. To eliminate genomic DNA, total RNA was treated with
649 RNase-free DNase I (Promega), and reverse-transcribed with a random hexamer or
650 oligo(dT)₂₄ primer using SYBR Premix ExTaq II (TaKaRa). qRT-PCR reactions were
651 performed with gene-specific forward and reverse primers using the PrimeScript RT-PCR
652 kit (TaKaRa) on the StepOne Real-Time PCR system (Applied Biosystems). The thermal
653 cycling program consisted of initial 30-second denaturation at 95°C followed by 40 cycles

654 of 5 seconds at 95°C and 30 seconds at 60°C. At the end of run, melting curves were
655 established for each PCR product to check the specificity of amplification. Expression
656 levels of mRNAs of interest were normalized relative to *TUBULIN4* (At5g44340)
657 expression. DNA fragments amplified from poly(A)⁺ transcripts of several genes including
658 *cob* were sequenced to check the occurrence of mitochondrial editing, which confirmed
659 that they are derived from the mitochondrial genome but not from their copies present in
660 chromosome 2 [50]. Experiments were performed in biological triplicates. Primers for the
661 qRT-PCR analysis are listed in table S1.

662 **PARN activity assay of recombinant RRD1**

663 The pHAT plasmids in which the RRD1 or hPARN sequence had been inserted were
664 transformed into the Rosetta-gami 2 strain or the M15 strain of *E. coli*. Colonies were
665 grown overnight at 37°C in LB medium containing 100 µg ml⁻¹ ampicillin and 25 µg ml⁻¹
666 chloramphenicol for Rosetta-gami 2 and 100 µg ml⁻¹ ampicillin and 25 µg ml⁻¹ kanamycin
667 for M15. The cultures were diluted (6:100) in the same medium and grown at 37°C for
668 approximately 3 hours to reach OD₆₀₀ of 0.3 to 0.4, and then treated with 0.2 mM isopropyl
669 β-D-1-thiogalactopyranoside (IPTG) overnight at 18°C to induce the production of the his-
670 tagged RRD1 and hPARN proteins. After cell lysis, the proteins were purified by TALON
671 Metal Affinity Resin (Clontech) and filtered with Amicon Ultra 0.5ml (30K; Merck
672 Millipore). For the ribonuclease activity assay, the purified proteins (0.125 mg) or RNase
673 If (1.25 U; NEB) were incubated at 25°C for 60 minutes with a fluorescent-labeled RNA
674 substrate (5'-fluorescein isothiocyanate (FITC)-CUUUUAG(A₂₀); this sequence was
675 derived from the 3' extremity of *cox1* mRNA (Fig. 3C)) in 10 µL of reaction medium (1.5
676 mM MgCl₂, 100 mM KCl, 0.1 U RNasin Ribonuclease Inhibitor (Promega), 20 mM
677 HEPES-KOH (pH 7.0), 0.2 mM EDTA, 0.25 mM dithiothreitol, 10% (v/v) glycerol, 0.1%
678 BSA) [51]. The reaction was stopped by adding an equal volume of gel loading mix (90%
679 formamide, 0.5% (w/v) EDTA, 0.025% (w/v) bromophenol blue) and heating to 90°C for
680 3 minutes before cooling on ice. The reaction mixtures were loaded onto a 7 M urea-16%
681 polyacrylamide gel and separated by electrophoresis.

682 **CR-RT PCR analysis of the 3' end of mRNA**

683 CR-RT PCR analysis was performed principally according to [27]. Total RNA was
684 extracted with TRIzol reagent (Invitrogen) from seedlings that had been cultured for 7 days
685 at 22°C and then 2 days at 28°C. To eliminate genomic DNA, total RNA was treated with
686 DNase I (RT grade; Nippon Gene). Next 1 µg of total RNA was circularized with T4 RNA
687 ligase (Promega), desalted with Amicon Ultra 0.5ml (10K; Merck Millipore), and then
688 reverse-transcribed with a *cox1* specific primer (Atcox1-1; table S1) using M-MLV
689 (Moloney Murine Leukemia Virus) Reverse Transcriptase (RNase H minus, point mutant;
690 Promega). The RNA template was degraded by adding 1/5 volume of 1 M NaOH to the
691 reaction mixture and incubating at room temperature for 10 minutes. The solution was
692 neutralized by adding 1 M HCl and the cDNA was purified with the illustra GFX PCR
693 DNA and Gel Band Purification Kit (GE Healthcare). The 5'-3' junction sequence was
694 amplified by PCR with *cox1* specific primers Atcox1-5'(-176..-196) and Atcox1-
695 3'(+17..+38) using Ex Taq Hot Start Version (Takara). The thermal cycling program
696 consisted of initial 4 minute-denaturation at 95°C, followed by 40 cycles of 20 seconds at
697 95°C, 20 seconds at 50°C, and 40 seconds at 72°C. The PCR products were purified with
698 the Wizard SV Gel and PCR Clean-Up System (Promega) and cloned into the pGEM-T
699 Easy Vector (Promega) using DNA Ligation Kit <Mighty Mix> (Takara). The constructed
700 vector was transformed into the DH5α strain of *E. coli*, and about 20 clones were sequenced.
701 Primers for the CR RT-PCR analysis are listed in table S1.

702 **Analysis of mitochondrial mRNA editing**

703 For the analysis of mitochondrial mRNA editing, total RNA was extracted with TRIzol
704 reagent (Invitrogen) from explants LR-induced at 28°C for 12 hours. Total RNA was
705 treated with RNase-free DNase I (Promega), and reverse-transcribed with a random
706 hexamer using the PrimeScript II 1st strand cDNA Synthesis kit (TaKaRa). Gene specific
707 primers were used to amplify cDNA by PCR using Ex Taq Hot Start Version (Takara). The
708 thermal cycling program consisted of initial 4-minute denaturation at 95°C followed by 30
709 to 40 cycles of 30 seconds at 95°C, 30 seconds at 55°C, and 90 to 120 seconds at 72°C.

710 The PCR products were purified either by ExoStar DNA purification reagent (GE
711 Healthcare) or Wizard SV Gel and PCR Clean-Up System (Promega), and then sequenced.

712 **Analysis of mitochondrial protein**

713 Isolation of intact mitochondria was performed principally according to [52]. Seed-derived
714 callus cultured in liquid callus-inducing medium (CIM) [16,17] in the dark with gentle
715 shaking was used as starting material. About 16 g of callus was homogenized in 40 ml ice-
716 cold grinding buffer (0.3 M Mannitol, 50 mM Tetrasodium pyrophosphate, 2 mM EDTA
717 (Disodium salt), 0.5 % (w/v) PVP-40, 0.5 % (w/v) BSA, 20 mM L-cysteine, pH 8.0 (HCl))
718 with a mortar, pestle, and glass beads (0.4-mm diameter). The homogenate was filtered
719 through four layers of Miracloth (Millipore) and centrifuged at 2,300g for 5 minutes twice.
720 The resulting supernatant was centrifuged at 18,000g for 10 minutes. The resulting pellet
721 was resuspended in wash buffer (0.3 M Mannitol, 10 mM *N*-Tris(hydroxymethyl)methyl-
722 2-aminoethanesulfonic acid (TES), 0.1% (w/v) BSA, pH 7.5 (NaOH)) and layered over a
723 three-step Percoll (GE Healthcare) gradient (40%, 21%, and 16% (v/v)). The gradient was
724 centrifuged at 23,500 rpm (approximately 40,000g to 70,000g) for 30 minutes.
725 Mitochondria were collected from the 21% and 40% interface and washed twice in wash
726 buffer (without BSA) by centrifugation at 18,000g for 10 minutes.

727 For BN-PAGE analysis, 10 µg protein of mitochondria was solubilized in 12 µL Native
728 PAGE Sample Buffer (1% n-dodecyl-β-D-maltoside (DDM), Thermo Fisher Scientific),
729 mixed with 1.8 µL of sample additive (33.3% (w/v) glycerol, 1.67% (w/v) Coomassie
730 Brilliant Blue (CBB) G250), and then separated by electrophoresis on a NativePAGE 4 to
731 16%, Bis-Tris Gel (Thermo Fisher Scientific).

732 For immunoblot analysis, proteins separated via SDS-PAGE were transferred to a
733 PVDF membrane and exposed to a primary antibody against cyt c (AS08 343A, Agrisera;
734 1:5000 dilution). As a secondary antibody, we used a peroxidase-labeled anti-rabbit
735 antibody (NIF824, GE Healthcare; 1:5000 dilution). Immunodetection was performed by
736 incubating the membranes in the Western BLoT Quant HRP Substrate (Takara) and
737 recording the chemiluminescence by LuminoGraph I (ATTO).

738 **Graph drawing**

739 Bar charts were drawn using KaleidaGraph (Abelbeck Software) or Excel for Mac
740 (Microsoft). Scatter plots were drawn using KaleidaGraph or R software. Dot plots were
741 drawn using R software. Violin plots were overlaid using the `geom_flat_violin` function
742 (<https://gist.github.com/JoachimGoedhart/98ec16c041aab8954083097796c2fe81>). Box
743 plots were drawn using R software.

746 Supplementary Materials

- 747 Fig. S1. Chromosome mapping of the TDF mutations, *rrd1*, *rrd2*, and *rid4-1*.
748 Fig. S2. Complementation analysis and allelism test for the identification of the TDF genes
749 RRD1, RRD2, and RID4.
750 Fig. S3. Identification and characterization of the *rid4-2* mutant.
751 Fig. S4. Functionality and expression of *RRD1::RRD1:GFP* and *RID4::RID4:GFP*
752 Fig. S5. Characterization of RRD1 function.
753 Fig. S6. Sequence alignment of RRD1 and PARNs of various organisms.
754 Fig. S7. Comprehensive analysis of mitochondrial mRNA editing in *rrd2* and *rid4-1*.
755 Fig. S8. Analysis of mitochondrial mRNA editing in *rrd2* and *rid4-1*.
756 Fig. S9. Effects of NPA and PQ on LR formation.
757 Table S1. Primers used in this study.

758 References and Notes

- 759 1. Torres-Martínez, H.H., Rodríguez-Alonso, G., Shishkova, S., and Dubrovsky, J.G. (2019).
760 Lateral root primordium morphogenesis in angiosperms. *Front. Plant Sci.* *10*, 206.
761 2. Hammani, K., and Giegé, P. (2014). RNA metabolism in plant mitochondria. *Trends Plant*
762 *Sci.* *19*, 380–389.
763 3. von Wangenheim, D., Fangerau, J., Schmitz, A., Smith, R.S., Leitte, H., Stelzer, E.H.K.,
764 and Maizel, A. (2016). Rules and self-organizing properties of post-embryonic plant organ
765 cell division patterns. *Curr. Biol.* *26*, 439–449.
766 4. Goh, T., Toyokura, K., Wells, D.M., Swarup, K., Yamamoto, M., Mimura, T., Weijers,
767 D., Fukaki, H., Laplace, L., Bennett, M.J., *et al.* (2016). Quiescent center initiation in the
768 *Arabidopsis* lateral root primordia is dependent on the *SCARECROW* transcription factor.
769 *Development* *143*, 3363–3371.
770 5. Lavenus, J., Goh, T., Roberts, I., Guyomarc'h, S., Lucas, M., De Smet, I., Fukaki, H.,
771 Beeckman, T., Bennett, M., and Laplace, L. (2013). Lateral root development in
772 *Arabidopsis*: fifty shades of auxin. *Trends Plant Sci.* *18*, 455–463.
773 6. Benková, E., Michniewicz, M., Sauer, M., Teichmann, T., Seifertová, D., Jürgens, G., and
774 Friml, J. (2003). Local, efflux-dependent auxin gradients as a common module for plant
775 organ formation. *Cell* *115*, 591–602.
776 7. Geldner, N., Richter, S., Vieten, A., Marquardt, S., Torres-Ruiz, R.A., Mayer, U., and
777 Jürgens, G. (2004). Partial loss-of-function alleles reveal a role for GNOM in auxin
778 transport-related, post-embryonic development of *Arabidopsis*. *Development* *131*, 389–
779 400.
780 8. De Smet, I., Lau, S., Voß, U., Vanneste, S., Benjamins, R., Rademacher, E.H., Schlereth,
781 A., De Rybel, B., Vassileva, V., Grunewald, W., *et al.* (2010). Bimodular auxin response
782 controls organogenesis in *Arabidopsis*. *Proc. Natl. Acad. Sci. U. S. A.* *107*, 2705–2710.
783 9. De Smet, I., Vassileva, V., De Rybel, B., Levesque, M.P., Grunewald, W., Van Damme,
784 D., Van Noorden, G., Naudts, M., Van Isterdael, G., De Clercq, R., *et al.* (2008).
785 Receptor-like kinase ACR4 restricts formative cell divisions in the *Arabidopsis* root.
786 *Science*. *322*, 594–597.
787 10. Murphy, E., Vu, L.D., den Broeck, L., Lin, Z.F., Ramakrishna, P., van de Cotte, B.,
788 Gaudinier, A., Goh, T., Slane, D., Beeckman, T., *et al.* (2016). RALFL34 regulates
789 formative cell divisions in *Arabidopsis* pericycle during lateral root initiation. *J. Exp. Bot.*
790 *67*, 4863–4875.
791 11. Hirota, A., Kato, T., Fukaki, H., Aida, M., and Tasaka, M. (2007). The auxin-regulated
792 AP2/EREBP gene PUCHI is required for morphogenesis in the early lateral root
793 primordium of *Arabidopsis*. *Plant Cell* *19*, 2156–2168.

- 794 12. Du, Y.J., and Scheres, B. (2017). PLETHORA transcription factors orchestrate de novo
795 organ patterning during *Arabidopsis* lateral root outgrowth. *Proc. Natl. Acad. Sci. U. S. A.*
796 *114*, 11709–11714.
- 797 13. Benitez-Alfonso, Y., Faulkner, C., Pendle, A., Miyashima, S., Helariutta, Y., and Maule,
798 A. (2013). Symplastic intercellular connectivity regulates lateral root patterning. *Dev. Cell*
799 *26*, 136–147.
- 800 14. Napsucially-Mendivil, S., Alvarez-Venegas, R., Shishkova, S., and Dubrovsky, J.G.
801 (2014). *ARABIDOPSIS HOMOLOG of TRITHORAX1 (ATX1)* is required for cell
802 production, patterning, and morphogenesis in root development. *J. Exp. Bot.* *65*, 6373–
803 6384.
- 804 15. Vermeer, J.E.M., von Wangenheim, D., Barberon, M., Lee, Y., Stelzer, E.H.K., Maizel,
805 A., and Geldner, N. (2014). A spatial accommodation by neighboring cells is required for
806 organ initiation in *Arabidopsis*. *Science*. *343*, 178–183.
- 807 16. Sugiyama, M. (2003). Isolation and initial characterization of temperature-sensitive
808 mutants of *Arabidopsis thaliana* that are impaired in root redifferentiation. *Plant Cell*
809 *Physiol.* *44*, 588–596.
- 810 17. Konishi, M., and Sugiyama, M. (2003). Genetic analysis of adventitious root formation
811 with a novel series of temperature-sensitive mutants of *Arabidopsis thaliana*.
812 *Development* *130*, 5637–5647.
- 813 18. Otsuka, K., and Sugiyama, M. (2012). Tissue organization of fasciated lateral roots of
814 *Arabidopsis* mutants suggestive of the robust nature of outer layer patterning. *J. Plant Res.*
815 *125*, 547–554.
- 816 19. Ohtani, M., Demura, T., and Sugiyama, M. (2010). Particular significance of SRD2-
817 dependent snRNA accumulation in polarized pattern generation during lateral root
818 development of *Arabidopsis*. *Plant Cell Physiol.* *51*, 2002–2012.
- 819 20. Hu, Z.B., Vanderhaeghen, R., Cools, T., Wang, Y., De Clercq, I., Leroux, O., Nguyen, L.,
820 Belt, K., Millar, A.H., Audenaert, D., *et al.* (2016). Mitochondrial defects confer tolerance
821 against cellulose deficiency. *Plant Cell* *28*, 2276–2290.
- 822 21. Pavlopoulou, A., Vlachakis, D., Balatsos, N.A.A., and Kossida, S. (2013). A
823 comprehensive phylogenetic analysis of deadenylases. *Evol. Bioinforma.* *9*, 491–497.
- 824 22. Lee, D., Park, D., Park, J.H., Kim, J.H., and Shin, C. (2019). Poly(A)-specific
825 ribonuclease sculpts the 3' ends of microRNAs. *RNA* *25*, 388–405.
- 826 23. Hirayama, T., Matsuura, T., Ushiyama, S., Narusaka, M., Kurihara, Y., Yasuda, M.,
827 Ohtani, M., Seki, M., Demura, T., Nakashita, H., *et al.* (2013). A poly(A)-specific
828 ribonuclease directly regulates the poly(A) status of mitochondrial mRNA in *Arabidopsis*.
829 *Nat. Commun.* *4*.
- 830 24. Kanazawa, M., Ikeda, Y., Nishihama, R., Yamaoka, S., Lee, N.H., Yamato, K.T., Kohchi,
831 T., and Hirayama, T. (2020). Regulation of the poly(A) status of mitochondrial mRNA by
832 poly(A)-specific ribonuclease is conserved among land plants. *Plant Cell Physiol.* *61*,
833 470–480.
- 834 25. Hirayama, T. (2014). A unique system for regulating mitochondrial mRNA poly(A) status
835 and stability in plants. *Plant Signal. Behav.* *9*, 1–4.
- 836 26. Holec, S., Lange, H., Canaday, J., and Gagliardi, D. (2008). Coping with cryptic and
837 defective transcripts in plant mitochondria. *Biochim. Biophys. Acta* *1779*, 566–573.
- 838 27. Forner, J., Weber, B., Thuss, S., Wildum, S., and Binder, S. (2007). Mapping of
839 mitochondrial mRNA termini in *Arabidopsis thaliana*: t-elements contribute to 5' and 3'
840 end formation. *Nucleic Acids Res.* *35*, 3676–3692.
- 841 28. Sallés, F.J., Richards, W.G., and Strickland, S. (1999). Assaying the polyadenylation state
842 of mRNAs. *Methods-a Companion to Methods Enzymol.* *17*, 38–45.

- 843 29. Reverdatto, S. V., Dutko, J.A., Chekanova, J.A., Hamilton, D.A., and Belostotsky, D.A.
844 (2004). mRNA deadenylation by PARN is essential for embryogenesis in higher plants.
845 *RNA* *10*, 1200–1214.
- 846 30. Barkan, A., and Small, I. (2014). Pentatricopeptide Repeat Proteins in Plants. *Annu. Rev.*
847 *Plant Biol.* *65*, 415–442.
- 848 31. Kobayashi, T., Yagi, Y., and Nakamura, T. (2019). Comprehensive prediction of target
849 RNA editing sites for PLS-class PPR proteins in *Arabidopsis thaliana*. *Plant Cell Physiol.*
850 *60*, 862–874.
- 851 32. Cheng, S.F., Gutmann, B., Zhong, X., Ye, Y.T., Fisher, M.F., Bai, F.Q., Castleden, I.,
852 Song, Y., Song, B., Huang, J.Y., *et al.* (2016). Redefining the structural motifs that
853 determine RNA binding and RNA editing by pentatricopeptide repeat proteins in land
854 plants. *Plant J.* *85*, 532–547.
- 855 33. Giegé, P., Grienenberger, J.M., and Bonnard, G. (2008). Cytochrome c biogenesis in
856 mitochondria. *Mitochondrion* *8*, 61–73.
- 857 34. Heazlewood, J.L., Whelan, J., and Millar, A.H. (2003). The products of the mitochondrial
858 *orf25* and *orfB* genes are Fo components in the plant F1Fo ATP synthase. *Febs Lett.* *540*,
859 201–205.
- 860 35. Takenaka, M., Jörg, A., Burger, M., and Haag, S. (2019). RNA editing mutants as
861 surrogates for mitochondrial SNP mutants. *Plant Physiol. Biochem.* *135*, 310–321.
862 Available at: <https://doi.org/10.1016/j.plaphy.2018.12.014>.
- 863 36. Pasternak, T., Potters, G., Caubergs, R., and Jansen, M.A.K. (2005). Complementary
864 interactions between oxidative stress and auxins control plant growth responses at plant,
865 organ, and cellular level. *J. Exp. Bot.* *56*, 1991–2001.
- 866 37. Willems, P., Mhamdi, A., Stael, S., Storme, V., Kerchev, P., Noctor, G., Gevaert, K., and
867 Van Breusegem, F. (2016). The ROS wheel: refining ROS transcriptional footprints. *Plant*
868 *Physiol.* *171*, 1720–1733.
- 869 38. Potters, G., Pasternak, T.P., Guisez, Y., and Jansen, M.A.K. (2009). Different stresses,
870 similar morphogenic responses: integrating a plethora of pathways. *Plant Cell Environ.*
871 *32*, 158–169.
- 872 39. Huang, S.B., Van Aken, O., Schwarzländer, M., Belt, K., and Millar, A.H. (2016). The
873 roles of mitochondrial reactive oxygen species in cellular signaling and stress response in
874 plants. *Plant Physiol.* *171*, 1551–1559.
- 875 40. Van Aken, O., Whelan, J., and Van Breusegem, F. (2010). Prohibitins: mitochondrial
876 partners in development and stress response. *Trends Plant Sci.* *15*, 275–282. Available at:
877 <http://dx.doi.org/10.1016/j.tplants.2010.02.002>.
- 878 41. Arimura, S., and Tsutsumi, N. (2002). A dynamin-like protein (ADL2b), rather than FtsZ,
879 is involved in *Arabidopsis* mitochondrial division. *Proc. Natl. Acad. Sci. U. S. A.* *99*,
880 5727–5731.
- 881 42. Ulmasov, T., Murfett, J., Hagen, G., and Guilfoyle, T.J. (1997). Aux/IAA Proteins repress
882 expression of reporter genes containing natural and highly active synthetic auxin response
883 elements. *Plant Cell* *9*, 1963–1971.
- 884 43. Malamy, J.E., and Benfey, P.N. (1997). Organization and cell differentiation in lateral
885 roots of *Arabidopsis thaliana*. *Development* *124*, 33–44.
- 886 44. Ueda, T., Yamaguchi, M., Uchimiya, H., and Nakano, A. (2001). Ara6, a plant-unique
887 novel type Rab GTPase, functions in the endocytic pathway of *Arabidopsis thaliana*.
888 *EMBO J.* *20*, 4730–4741.
- 889 45. Kato, A., Maki, K., Ebina, T., Kuwajima, K., Soda, K., and Kuroda, Y. (2007). Mutational
890 analysis of protein solubility enhancement using short peptide tags. *Biopolymers* *85*, 12–
891 18.

- 892 46. Clough, S.J., and Bent, A.F. (1998). Floral dip: a simplified method for *Agrobacterium*-
893 mediated transformation of *Arabidopsis thaliana*. *Plant J.* 16, 735–743.
- 894 47. Martinez-Trujillo, M., Limones-Briones, V., Cabrera-Ponce, J.L., and Herrera-Estrella, L.
895 (2004). Improving transformation efficiency of *Arabidopsis thaliana* by modifying the
896 floral dip method. *Plant Mol. Biol. Report.* 22, 63–70.
- 897 48. Kohl, M., and Deigner, H.P. (2010). Preprocessing of gene expression data by optimally
898 robust estimators. *BMC Bioinformatics* 11.
- 899 49. Del Carratore, F., Jankevics, A., Eisinga, R., Heskes, T., Hong, F., and Breitling, R.
900 (2017). RankProd 2.0: a refactored bioconductor package for detecting differentially
901 expressed features in molecular profiling datasets. *Bioinformatics* 33.
- 902 50. Stupar, R.M., Lilly, J.W., Town, C.D., Cheng, Z., Kaul, S., Buell, C.R., and Jiang, J.M.
903 (2001). Complex mtDNA constitutes an approximate 620-kb insertion on *Arabidopsis*
904 *thaliana* chromosome 2: implication of potential sequencing errors caused by large-unit
905 repeats. *Proc. Natl. Acad. Sci. U. S. A.* 98, 5099–5103.
- 906 51. Cheng, Y., Liu, W.-F., Yan, Y.-B., and Zhou, H.-M. (2005). A nonradioactive assay for
907 poly(A)-specific ribonuclease activity by methylene blue colorimetry. *Protein Pept. Lett.*
908 13, 125–128.
- 909 52. Murcha, M.W., and Whelan, J. (2015). Isolation of intact mitochondria from the model
910 plant species *Arabidopsis thaliana* and *Oryza sativa*. In *Methods in Molecular Biology*
911 (Humana Press Inc.), pp. 1–12. Available at: http://link.springer.com/10.1007/978-1-4939-2639-8_1.

913
914

Acknowledgments

915 We thank Tsuyoshi Nakagawa for providing the binary vector pGW3, Mamoru Sugita for
916 valuable discussion on the PPR proteins, Hajime Sakurai for the technical support for the
917 expression of *35S::RRD2::GFP* in protoplasts, Shin-ichi Arimura for providing the
918 *35S::Mt-GFP* line, Yuta Otsuka and Yuki Kondo for the assistance on GFP imaging,
919 Yukiko Sugisawa for the technical support for microarray data collection, Hatsune
920 Morinaka for the assistance on qRT-PCR, and Tom J. Guilfoyle for providing the
921 *DR5::GUS* line, and the RIKEN BioResource Research Center for providing the hPARN
922 cDNA clone. **Funding:** This work was supported by Grant-in-Aid for Scientific Research
923 on Priority Areas (No. 19060001 to M.S.), the Graduate Program for Leaders in Life
924 Innovation (GPLLI) at the University of Tokyo Life Innovation Leading Graduate School
925 (for A.M.) from the Ministry of Education, Culture, Sports, Science and Technology, Japan
926 (MEXT), and by Grant-in-Aid for Scientific Research (B) (No. 25291057 to M.S.) and
927 Grants-in-Aid for JSPS Fellows (No. 09J08676 to K.O. and No. 17J05722 to A.M.) from
928 Japan Society for the Promotion of Science (JSPS). **Author contributions:** K.O. designed
929 and performed experiments and data analysis mostly in the first half of this study, including
930 histological analysis of fasciated LR, positional cloning of *RRD1* and *RRD2*, construction
931 of the reporter genes, subcellular localization analysis of the TDF proteins, microarray data
932 collection, initial analysis of the poly(A) status of mitochondrial mRNAs, and initial
933 pharmacological analysis with respiratory inhibitors. A.M. designed and performed
934 experiments and data analysis mostly in the latter half of this study, including expression
935 analysis of the TDF genes, microarray data mining, analysis of polyadenylation and editing
936 of mitochondrial mRNAs, genetic analysis with *ags1*, analysis of mitochondrial proteins,
937 and pharmacological analysis with respiration- and ROS-related drugs. M.K. identified
938 *RID4* by positional cloning. M.N. designed and performed analysis of PARN activity of
939 recombinant RRD1. A.K. conducted chromosome mapping of *rrd1* and some of the initial
940 characterization of the TDF phenotype. H.T. isolated the *rid4-2* mutant. M.A. and M.Sa.
941 conducted chromosome mapping of *rid4-2*. K.Y. collected preliminary data on the genetic

942 relationship between *rrd1* and *ags1*. T.Ha. and K.N. contributed to the research design and
943 data interpretation for mitochondrial respiration-related analysis. T.U. contributed to the
944 research design, imaging analysis of GFP reporters, and data interpretation for subcellular
945 localization. Y.Y., T.N., and K.Y. performed preliminary analysis of RNA editing. Y.Y.,
946 T.K., and T.N. contributed to the research design and data interpretation for RNA editing-
947 related analysis. Y.S. contributed to the analysis of the recombinant RRD1 protein. T.Hi.
948 contributed to the research design and data interpretation for RNA metabolism-related
949 analysis. M.Su. launched and directed the study and conducted preliminary analyses. K.O.,
950 A.M., and M.Su. wrote the manuscript. All authors read and approved the paper.
951 **Competing interests:** The authors declare no competing financial interests. **Data and**
952 **materials availability:** The microarray data has been deposited in the Gene Expression
953 Omnibus (<http://www.ncbi.nlm.nih.gov/geo/>) under accession number GSE34595. All
954 data needed to evaluate the conclusions in the paper are present in the paper and/or the
955 Supplementary Materials. Plant materials used in this study can be distributed upon request
956 to the corresponding author.
957

958 **Figures and Tables**

959

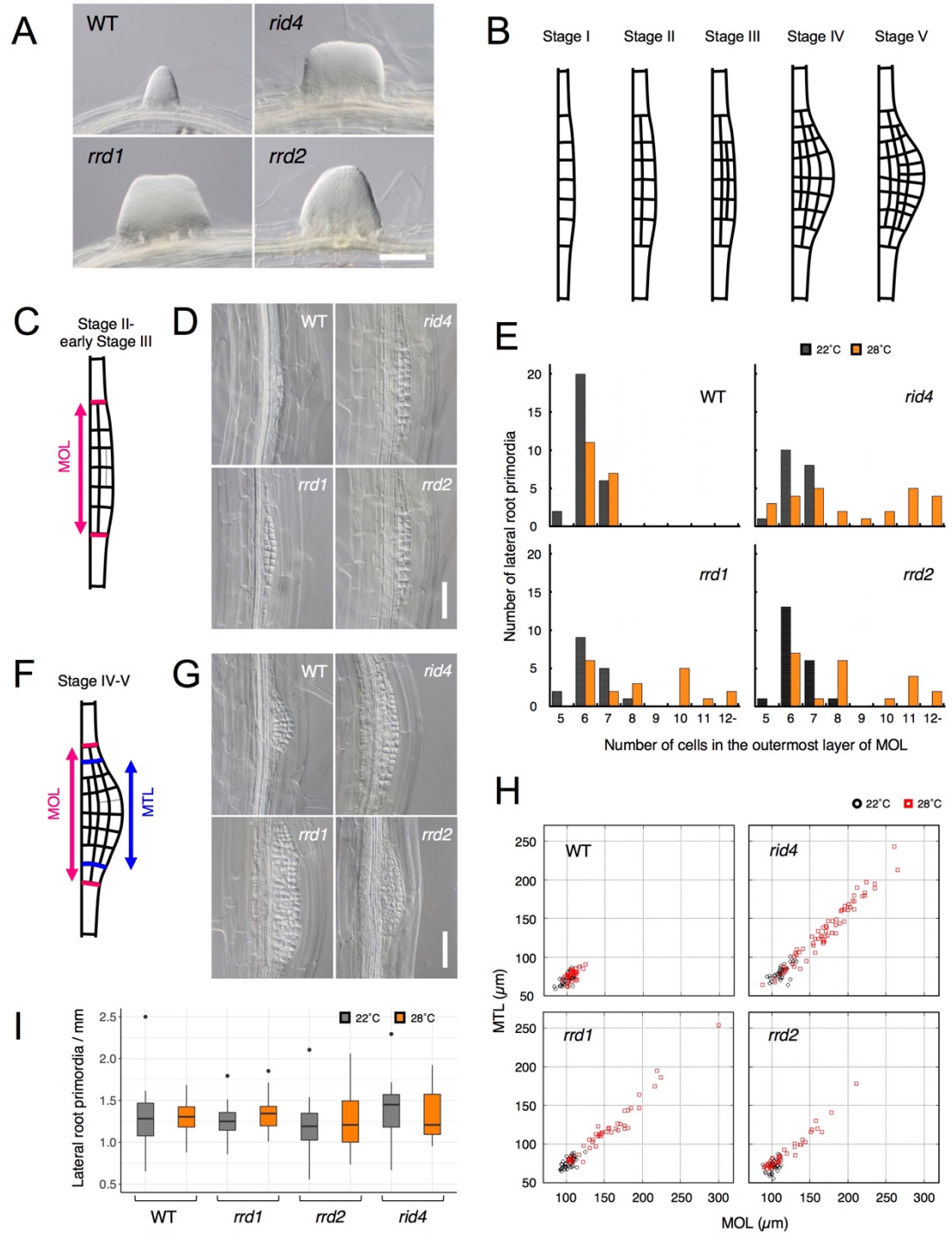


Fig. 1

960

961

962

963 **Fig. 1 Effects of the TDF mutations on the early stages of LR development.** (A) Fasciated LRs
964 formed at 28°C in the TDF mutant explants vs. a normal root on the wild-type (WT) explant after
965 6 days of culture. (B) Schematic representation of LR development (stages I–V). (C) Schematic
966 image of a primordium at stage II. The area consisting of more than one cell layer (MOL) is
967 delimited by red lines. (D) Stage II primordia formed at 28°C in WT and TDF mutant explants.
968 (E) Effects of the TDF mutations on the number of cells in the outermost layer of the MOL area
969 of stage II primordia at 22°C (black) and 28°C (orange). N = 17–28. (F) Schematic image of a
970 primordium at the transition from stage IV to stage V. The areas consisting of MOL and more than
971 two cell layers (MTL) are delimited by red lines and blue lines, respectively. (G) Stage IV–V
972 primordia formed at 28°C in WT explants and TDF mutant explants. (H) Scatterplot of the effect
973 of the TDF mutations on the width of the MTL vs. the width of the MOL areas at 22°C (black)
974 and 28°C (red). N = 31–66. (I) LR densities in the WT explants and TDF mutant explants cultured
975 at 22°C or 28°C (including all developmental stages; median, 25%–75% quantile, N = 21–29, $P >$
976 0.3, Kruskal-Wallis test). Scale bars, 100 μm (A), 50 μm (D, G).

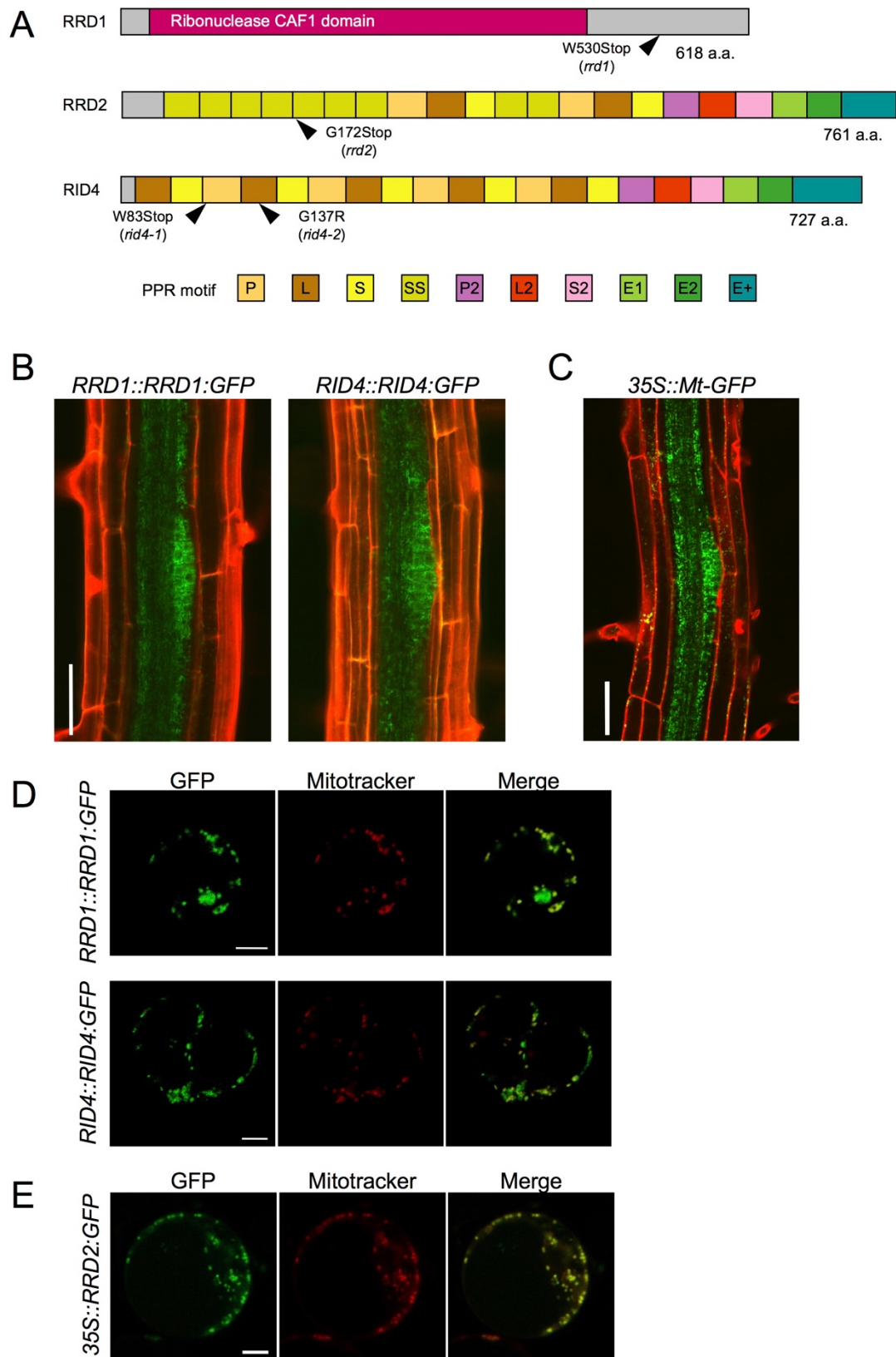


Fig. 2

978
979
980
981
982
983
984

Fig. 2 Tissue-specific expression and subcellular localization of the TDF proteins. (A) Structures of the RRD1, RRD2, and RID4 proteins. **(B and C)** Expression of *RRD1::RRD1:GFP* (**B**, left), *RID4::RID4:GFP* (**B**, right), and *35S::Mt-GFP* (**C**) at stage II of LR primordium development. Propidium iodide was used as a red counterstain. **(D and E)** Expression of *RRD1::RRD1:GFP* (**D**, upper panels), *RID4::RID4:GFP* (**D**, lower panels), and *35S::RRD2:GFP* (**E**) in callus-derived protoplasts. Mitochondria were labeled with MitoTracker Orange. Scale bars, 50 μm (**B and C**) and 5 μm (**D and E**).

985

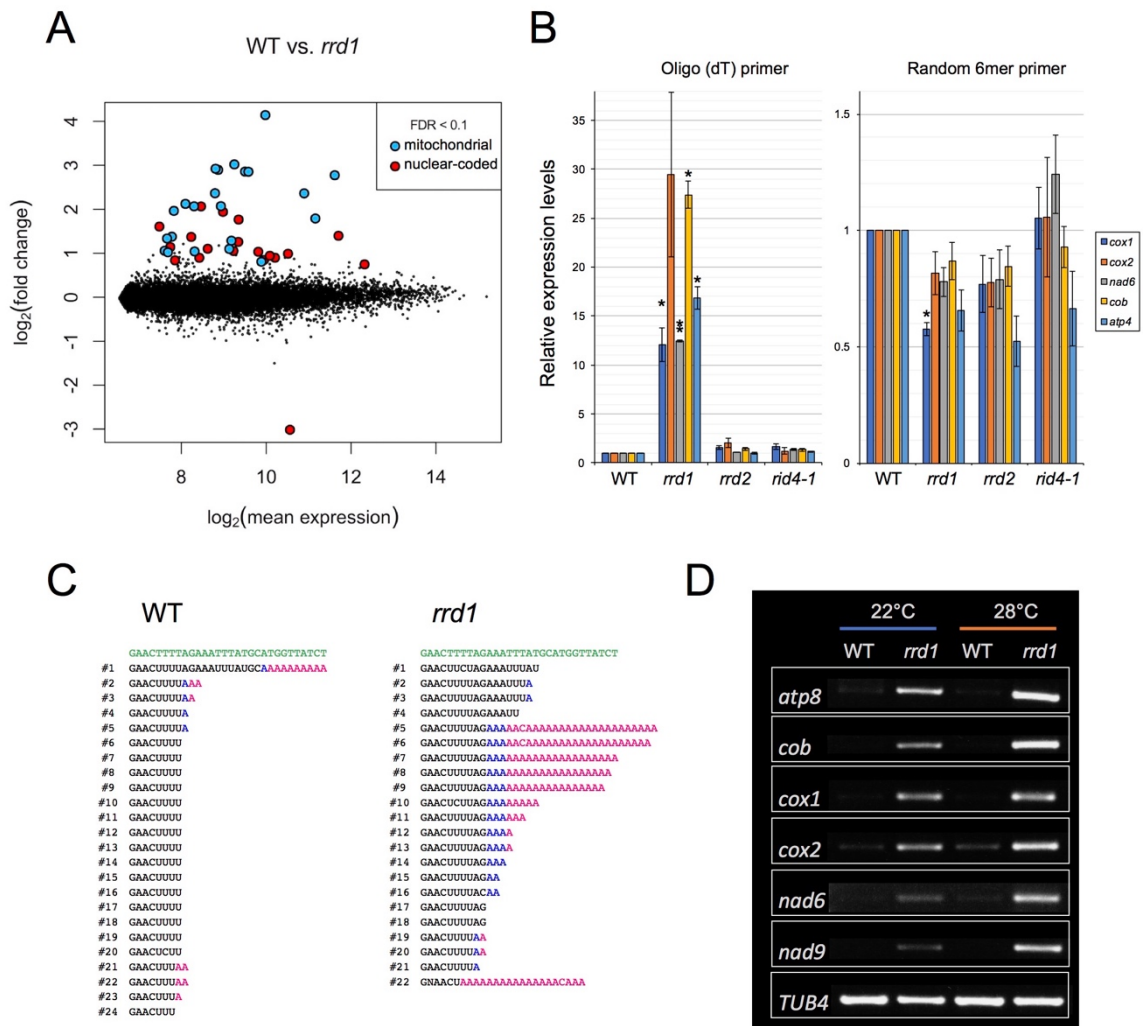


Fig. 3

Fig. 3 Accumulation of polyadenylated mitochondrial transcripts in *rrd1*. (A) MA plot for the microarray analysis of poly(A)⁺ transcripts of *rrd1* vs. wild-type (WT) explants in which LR_s were induced at 28°C for 12 hours. (B) qRT-PCR analysis of explants in which LR_s were induced at 28°C for 12 hours. The total and polyadenylated transcript levels are shown for cytochrome oxidase subunit 1 (*cox1*), *cox2*, NADH dehydrogenase subunit 6 (*nad6*), apocytochrome B (*cob*), and ATP synthase subunit 4 (*atp4*) (mean ± s.d., N = 3, *P < 0.05, **P < 0.01, 1 sample *t* test with Benjamini-Hochberg correction). (C) Analysis of the 3' end of the *cox1* mRNA by CR-RT PCR. mRNAs were prepared from WT and *rrd1* seedlings that were first grown at 22°C for 7 days, and then at 28°C for 2 days. The genomic sequence of *cox1* is shown in green. (D) RACE-PAT assay showing the accumulation of polyadenylated transcripts of *atp8*, *cob*, *cox1*, *cox2*, *nad6*, *nad9*, and *TUB4*. mRNAs were prepared from explants in which LR_s were induced at 22°C or 28°C for 12 hours.

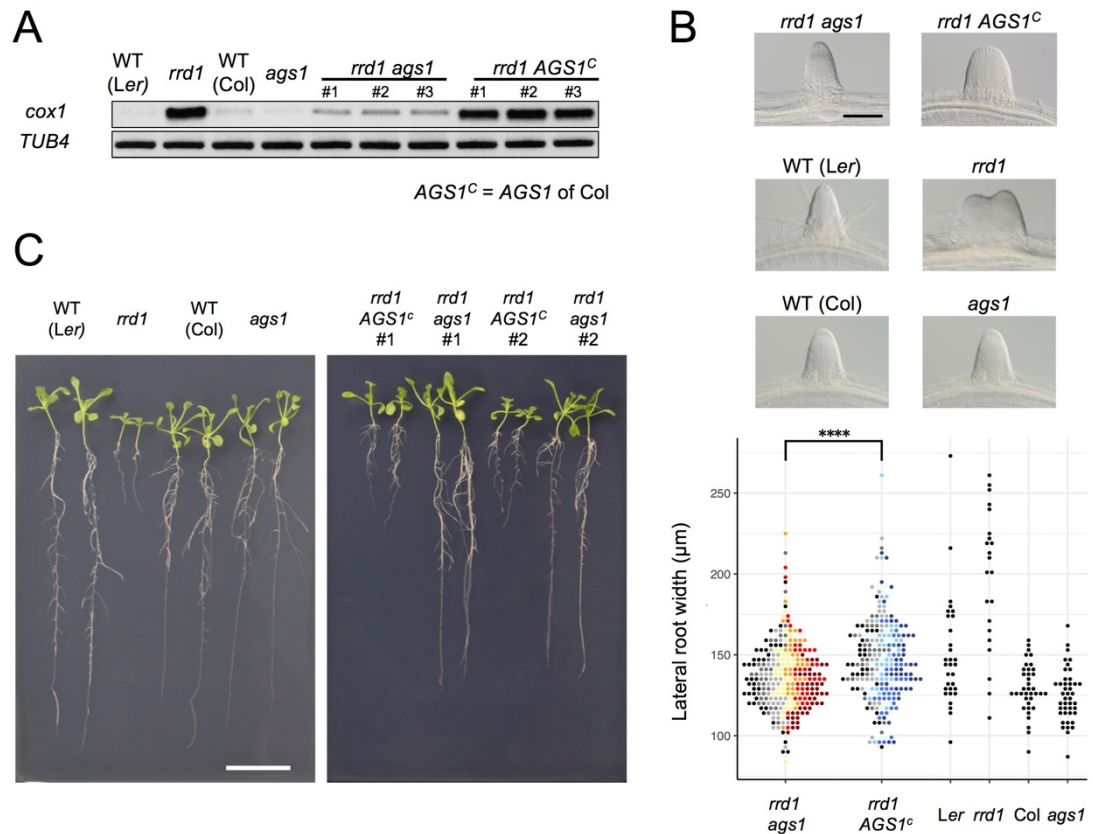


Fig. 4

Fig. 4 Effects of *ags1* on the phenotypes of *rrd1*. (A) RACE-PAT assay showing the accumulation of polyadenylated transcripts of *cox1* and *TUB4*. *rrd1* mutant strains harboring either *ags1* or *AGS1^c* (*AGS1* of Col background) were obtained by *rrd1* (Ler background) × *ags1* (Col background) and *rrd1* × Col crosses, respectively. mRNAs were prepared from seedlings that were first grown at 22°C for 5 days, and then at 28°C for 3 days. (B) Representative images of LR formed at 28°C after 6 days of culture (upper panels). The basal width of the LR that were formed in this way was scored (lower panel, N = 115–116 for *rrd1 ags1*, and *rrd1 AGS1^c*, N = 22–43 for others, *****P* < 10⁻⁴, Mann–Whitney–Wilcoxon test with Bonferroni correction). For *rrd1 ags1* and *rrd1 AGS1^c*, data were gathered from 7 strains, which are shown by different colors. (C) Seedlings grown at 28°C for 13 days on gellan gum plates. Scale bars, 100 μm (B) and 2 cm (C).

000
001
002
003
004
005
006
007
008
009
010
011

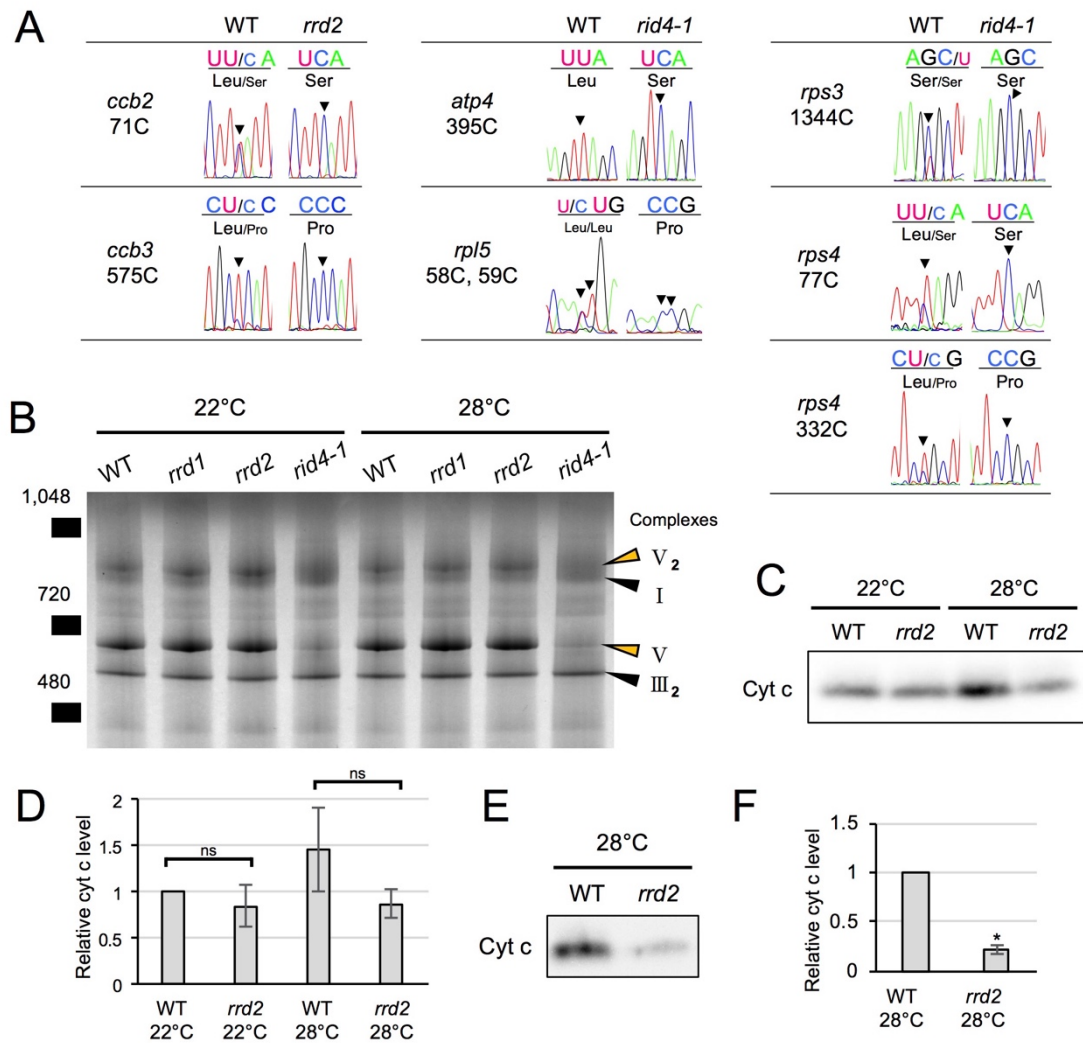


Fig. 5

Fig. 5 Effects of *rrd2* and *rid4* on mitochondrial mRNA editing and protein synthesis. (A) Sequencing analysis of mitochondrial mRNA editing in explants in which LR_s were induced at 28°C for 12 hours. (B) BN-PAGE analysis of mitochondrial protein complexes. Mitochondria were extracted from seed-derived liquid-cultured callus that were first incubated at 22°C for 20 days, and then at 22°C or 28°C for an additional 3 days. (C and D) Immunoblot analysis of cyt c. Mitochondria were extracted in the same conditions as in (B). The results of the densitometry analysis are shown in (D) (N = 3, mean ± s.d.). (E and F) Immunoblot analysis of cyt c using mitochondria extracted from callus that were cultured first at 22°C for 14 days, and then at 28°C for 7 days. The results of the densitometry analysis are shown in (F) (N = 2, mean ± s.d., **P < 0.01, Welch's *t* test)

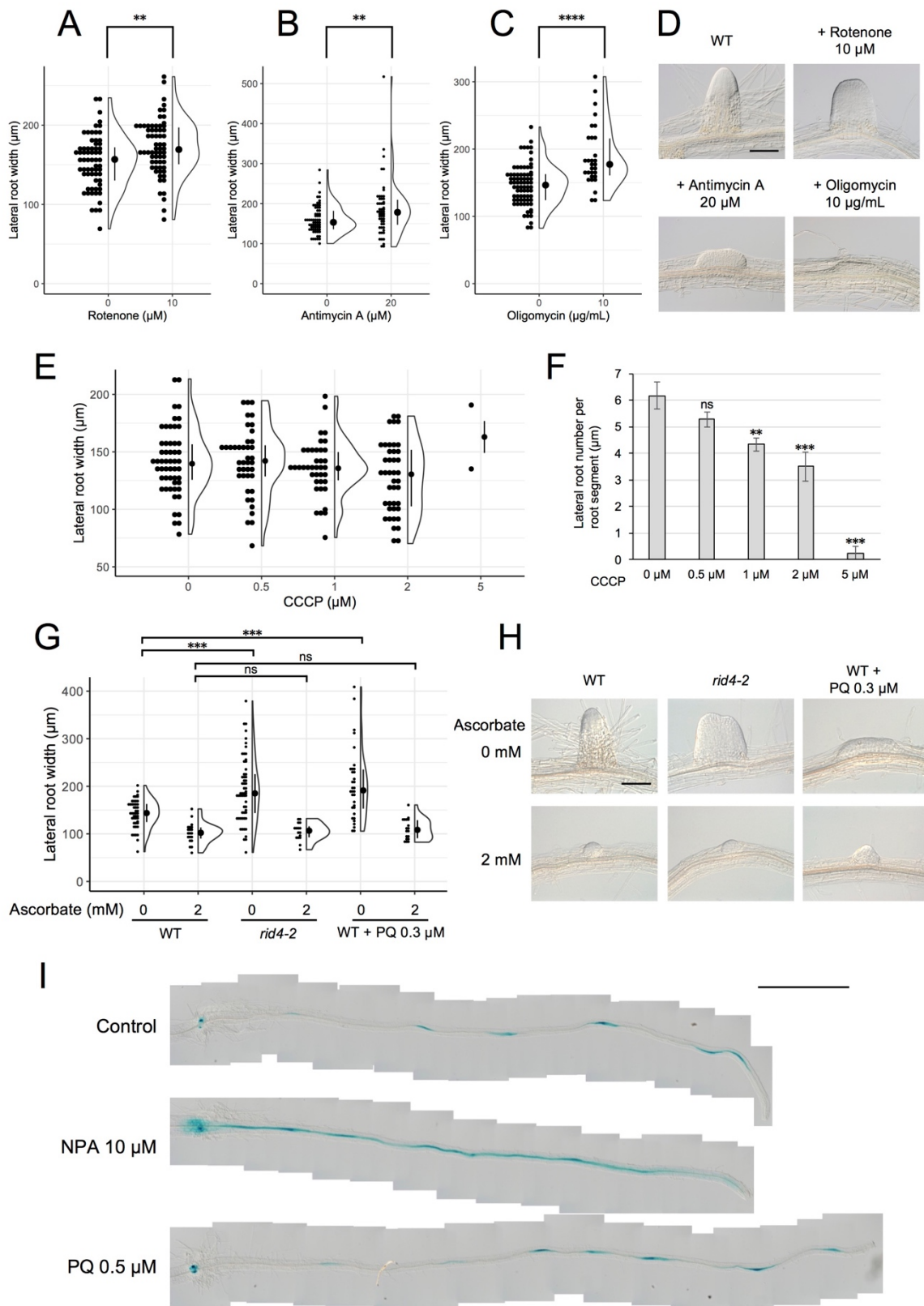


Fig. 6

024 **Fig. 6 Formation of fasciated LR**s after treatment with chemicals that inhibit
025 **mitochondrial respiration or induce ROS.** (A–D) LRs were induced at 28°C from the
026 wild-type (WT) plant in the presence of rotenone (A), antimycin A (B), or oligomycin (C),
027 and the basal width of the LRs that were formed was scored after 6 days in culture (median,
028 25%–75% quantile, N = 30–76, ***P* < 0.01, *****P* < 0.0001, Mann–Whitney–Wilcoxon
029 test). Typical LRs that were formed in each treatment are shown in (D). (E and F) LRs
030 were induced from the WT plant in the presence of CCCP. The basal width of LRs (E,
031 median, 25%–75% quantile, N = 2–53, *P* > 0.1, Kruskal-Wallis test) and the number of
032 LRs per segment (F, Number of segments = 12, ***P* < 0.01, ****P* < 0.001, Dunnett's test)
033 were scored on the 6th day. (G and H) The effects of the application of ascorbate on WT,
034 PQ-treated, or *rid4-2* segments during LR formation. The basal width of the LRs formed
035 was measured on the 6th day of LR induction (G, median, 25%–75% quantile, N = 16–58,
036 ****P* < 0.001, Mann–Whitney–Wilcoxon test with Bonferroni correction). Representative
037 images of LRs in each condition are shown in (H). (I) *DR5::GUS* expression at 12 hours
038 after LR induction under treatment with NPA or PQ. Scale bars, 100 μm (D and H) and 1
039 mm (I).

040
041 **Fig. S1 Chromosome mapping of the TDF mutations, *rrd1*, *rrd2*, and *rid4-1*.** (A)
042 Chromosome mapping of the *rrd1* mutation. The black rectangles represent annotation
043 units around the *RRD1* locus on chromosome 3, and the red numerals correspond to the
044 number of recombination events between DNA polymorphism markers and the *RRD1*
045 locus. The *rrd1* mutation was mapped to the region covered by the annotation units MJL12,
046 MTE24, and MWL2. Sequencing of this region, followed by complementation analysis,
047 identified the *rrd1* mutation as a G-to-A transition in At3g25430 (orange arrow). (B)
048 Chromosome mapping of the *rrd2* mutation. The black rectangles represent annotation
049 units around the *RRD2* locus on chromosome 1, and the red numerals correspond to the
050 number of recombination events between DNA polymorphism markers and the *RRD2*
051 locus. The *rrd2* mutation was mapped to the region covered by the annotation units F3C3,
052 F27G20, and F5D14. Sequencing of this region, followed by allelism analysis, identified
053 the *rrd2* mutation as a G-to-A transition in At1g32415 (orange arrow). (C) Chromosome
054 mapping of the *rid4-1* mutation. The black rectangles represent the annotation units around
055 the *RID4* locus on chromosome 2, and the red numerals correspond to the number of
056 recombination events between DNA polymorphism markers and the *RID4* locus. The *rid4*
057 mutation was mapped to the region covered by the annotation units F4P9 and T1B8.
058 Sequencing of this region, followed by complementation analysis, identified the *rid4*
059 mutation as a G-to-A transition in At2g33680 (orange arrow).

060 **Fig. S2 Complementation analysis and allelism test for the identification of the TDF**
061 **genes *RRD1*, *RRD2*, and *RID4*.** (A) Complementation analysis for the identification of
062 the *RRD1* gene. The genomic fragment GL07 encompassing At3g25430, where an *rrd1*
063 phenotype-linked mutation was found, was introduced into the wild-type (WT) plant,
064 which was then crossed with *rrd1*. Each individual of the F2 progeny was genotyped for
065 the *rrd1* allele and the GL07 transgene. Hypocotyl explants of the F2 progeny were
066 cultured on RIM at 28°C for 14 days and examined for adventitious rooting. The explants
067 were categorized according to the length of the ARs (Short, shorter than 5 mm; Long,
068 longer than 5 mm) and counted. The results showed that the development of ARs, which
069 was highly temperature sensitive in the *rrd1* mutant, was clearly rescued by the
070 introduction of GL07. Therefore, we concluded that the *RRD1* gene corresponds to

071 At3g25430. **(B and C)** Defect of AR formation in a T-DNA insertion mutant of At1g32415.
072 SALK_027874 carries a T-DNA insertion in the middle of At1g32415 **(B)**. The transcribed
073 region and open reading frame of At1g32415 are indicated by the open arrow and grey box,
074 respectively. Hypocotyl explants of Col, *Ler*, *rrd2*, and SALK_027874 were cultured on
075 RIM at 28°C for 27 days and examined for adventitious rooting **(C)**. The results indicated
076 that SALK_027874 and *rrd2* are defective in AR formation at this temperature. As AR
077 formation was not significantly affected at 22°C in both *rrd2* and SALK_027874 (data not
078 shown), SALK_027874 was shown to be temperature sensitive for root development, as
079 was *rrd2*. Bar, 1 cm. **(D)** Allelism test for the identification of the *RRD2* gene. The *rrd2*
080 mutant was crossed with SALK_027874 carrying a T-DNA insertion in At1g32415, in
081 which an *rrd2* phenotype-linked mutation was found. Each individual of the F2 progeny
082 was genotyped for the *rrd2* and the T-DNA insertion alleles. Hypocotyl explants of the F2
083 progeny were cultured on RIM at 28°C for 14 days and examined for adventitious rooting.
084 The explants were categorized according to the length of the ARs (Short, shorter than 5
085 mm; Long, longer than 5 mm) and counted. The results indicated clearly that *rrd2* and
086 SALK_027874 are allelic. Therefore, we concluded that the *RRD2* gene corresponds to
087 At1g32415. **(E)** Complementation analysis for the identification of the *RID4* gene. The
088 genomic fragment GL91321 encompassing At2g33680, where we found an *rid4*
089 phenotype-linked mutation, was introduced into *rid4*, and the resultant transgenic *rid4*
090 mutant harboring GL91321 (*rid4*/GL91321) was used for complementation analysis.
091 Hypocotyl explants of the WT plant, *rid4*, and *rid4*/GL91321-2 were cultured on RIM at
092 28°C for 19 days and examined for AR formation. The development of ARs, which was
093 highly temperature sensitive in the *rid4* mutant, was clearly rescued by the introduction of
094 GL91321. Therefore, we concluded that the *RID4* gene corresponds to At2g33680. Scale
095 bar, 1 cm.

096 **Fig. S3 Identification and characterization of the *rid4-2* mutant.** **(A)** Representative
097 images of LR formed at 22°C or 28°C in the explants of the wild-type plant or the *rid4-2*
098 mutant after 6 days of culture. Fasciated LR were observed in *rid4-2* explants at 28°C. **(B)**
099 Phenotypes of seedlings that were grown for 7 days on vertical agar plates. Seedlings were
100 grown either at 22°C or 28°C. **(C)** Allelism test between *rid4-1* and *rid4-2*. F₁ plants
101 derived from a reciprocal crossing between *rid4-1* and *rid4-2* were subjected to phenotypic
102 analysis regarding AR formation. Hypocotyl explants of *rid4-1*, *rid4-2*, *Ler* WT, and F₁
103 plants were cultured on RIM for 24 days at 28°C. **(D)** Chromosome mapping of the *rid4-2*
104 mutation. The black rectangles represent annotation units around the *RID4* locus on
105 chromosome 2, and the red numerals correspond to the number of recombination events
106 between DNA polymorphism markers and the *RID4* locus. *rid4-2* was mapped to the region
107 covered by the annotation units F4P9 and T29F13. Sequencing of this region, followed by
108 complementation analysis, identified the *rid4-2* mutation as a G-to-A transition in
109 At2g33680 (orange arrow). Scale bars, 100 μm **(A)** and 1 cm **(B)**.

110 **Fig. S4 Functionality and expression of *RRD1::RRD1:GFP* and *RID4::RID4:GFP*.** **(A)**
111 Phenotypic complementation of *rrd1* by the introduction of the GFP reporter gene
112 *RRD1::RRD1:GFP*. F₃ plants homozygous for *rrd1* derived from the cross between *rrd1*
113 and Col carrying *RRD1::RRD1:GFP* were phenotyped for AR formation from hypocotyl
114 explants at 28°C and genotyped for the presence of *RRD1::RRD1:GFP* (+, present; -,
115 absent). **(B)** Phenotypic complementation of *rid4* by the introduction of the GFP reporter
116 gene *RID4::RID4:GFP*. *rid4* homozygotes in which the genetic background had been
117 partially replaced by crossing with the Col strain were transformed with *RID4::RID4:GFP*.
118 Plants of the resultant T₂ line were phenotyped for AR formation from hypocotyl explants

119 at 28°C and genotyped for the presence of *RID4::RID4:GFP* (+, present; –, absent). **(C)**
120 Expression patterns of *RRD1* and *RID4* in the root apical region. GFP signals in the primary
121 roots of the transgenic plants harboring *RRD1::RRD1:GFP* and *RID4::RID4:GFP*
122 revealed strong expression of *RRD1* and *RID4* in the root apical meristem. Scale bar, 100
123 μm.

124 **Fig. S5 Characterization of RRD1 function.** **(A–C)** Microarray analysis of mitochondrial
125 genes in *rrd1*. MA plot for the microarray analysis of poly(A)⁺ transcripts of *rrd1* vs. wild-
126 type (WT) explants in which LR^s were induced at 28°C for 12 hours. The characterized
127 mitochondrial genes are shown in blue, while the noncharacterized mitochondrial ORFs or
128 pseudogenes are shown in red **(A)**. The names of the characterized genes are indicated in
129 **(B)**. **(C)** The function and array element ID of the characterized mitochondrial genes in the
130 GeneChip Arabidopsis Genome ATH1 Array. **(D and E)** PARN activity assay of RRD1.
131 TALON-purified fraction of the total cell lysate with or without IPTG induction **(D)**.
132 PARN activity assay using the TALON-purified fraction **(E)**.

133 **Fig. S6 Sequence alignment between RRD1 and PARNs from various organisms.** An
134 alignment of amino acid sequences was generated between RRD1 and PARNs from
135 humans, *Xenopus laevis*, and Arabidopsis using the ClustalW program and processed with
136 BOXSHADE (http://www.ch.embnet.org/software/BOX_form.html). Identical and
137 similar amino acid residues are highlighted on black and grey backgrounds, respectively.
138 The R3H domain is marked by the dotted orange box, and the RNA recognition motif
139 (RRM) is marked by the solid blue box. These domains are conserved in the animal PARNs
140 (human and *Xenopus laevis*), but are not clearly present in the Arabidopsis PARN and
141 RRD1. The pink asterisk represents the tryptophan codon that was changed to a stop codon
142 by the *rrd1* mutation. The red arrowheads represent the four residues that are important for
143 PARN activity (29).

144 **Fig. S7 Comprehensive analysis of mitochondrial mRNA editing in *rrd2* and *rid4-1*.** A
145 sequencing analysis of mitochondrial mRNA editing was performed using explants in
146 which LR^s were induced at 28°C for 12 hours. The color code indicates the level of C-to-
147 U RNA editing at each site (editing status: –0.5 = 100% C, 0.5 = 100% U). The presumptive
148 specific editing sites of RRD2 and RID4 are marked by solid black boxes. RNA editing in
149 *rid4-2* was also analyzed for sites affected in *rid4-1*.

150 **Fig. S8 Analysis of mitochondrial mRNA editing in *rrd2* and *rid4-1*.** **(A)** A sequencing
151 analysis of mitochondrial mRNA editing was performed using explants in which LR^s were
152 induced at 22°C for 12 hours. **(B)** Alignment of the estimated binding sequence of RRD2
153 and RID4 (31). **(C)** Analysis of the mRNA editing of *ccb3* in explants that were cultured
154 at 22°C or 28°C for 12 hours.

155 **Fig. S9 Effects of NPA and PQ on LR formation.** Root explants 6 days after LR
156 induction under treatment with NPA or PQ. Scale bar, 1 mm.

157 **Table S1. Primers used in this study.**

158